An algebraic non-equilibrium turbulence model of the high Reynolds number transition region

Nils T. Basse[a]

[a] *Independent Scientist*
Trubadurens väg 8, 423 41 Torslanda, Sweden

January 10, 2023

Abstract

We present a mixing length based algebraic turbulence model calibrated to pipe flow; the main purpose of the model is to capture the increasing turbulence production-to-dissipation ratio observed in connection with the high Reynolds number transition region.

The model includes the mixing length description by Gersten and Herwig which takes the observed variation of the von Kármán number with Reynolds number into account. Pipe wall roughness effects are included in the model.

Results are presented for area-averaged (integral) quantities which can be used both as a self-contained model and as initial inlet boundary conditions for computational fluid dynamics simulations.

1. Introduction

The impetus for this paper came from an invited presentation on boundary conditions for turbulence modelling [1]. Based on an observed variation of the turbulence production-to-dissipation ratio with Reynolds number, a corresponding variation of the turbulence model constant C_μ was discussed. Previously, Princeton Superpipe measurements [2, 3] of streamwise mean and fluctuating velocities have been analysed in detail [4, 5].

We present a new algebraic (zero-equation) turbulence model based on the Prandtl mixing length concept [6, 7] to improve our understanding of the observed high Reynolds number transition region. The model can be used both standalone and to provide initialisation of inlet boundary conditions

Email address: nils.basse@npb.dk (Nils T. Basse)

for computational fluid dynamics (CFD) simulations [8, 9]. Our approach is similar to the "LIKE" algorithm in [10], where the letters in the abbreviation represent the integral turbulent **L**ength scale, turbulence **I**ntensity, turbulent **K**inetic energy and turbulent dissipation rate ε (**E**).

The paper is organised as follows: In Section 2, we summarise previous relevant findings, followed by a description of the basic model in Section 3. The turbulent viscosity ratio is discussed in Section 4, mixing length scales are covered in Section 5 and turbulence intensity definitions are presented in Section 6. Results from our new model are provided in Section 7 and discussed in Section 8. We conclude and propose future research directions in Section 9.

2. The high Reynolds number transition region

In this section we summarise earlier findings which prompted this study. We begin by defining the friction Reynolds number:

$$Re_\tau = \frac{u_\tau \delta}{\nu_{\text{kin}}}, \tag{1}$$

where u_τ is the friction velocity, δ is the boundary layer thickness (pipe radius R for pipe flow) and ν_{kin} is the kinematic viscosity.

The normalised mean velocity U is given by the log-law [11, 4]:

$$\frac{U_{\text{g,mean}}(z)}{u_\tau} = \frac{1}{\kappa_g}\log(z^+) + A_{\text{g,mean}}, \tag{2}$$

where the subscript "g" indicates "global", $A_{\text{g,mean}} = 1.01$ and the global von Kármán number κ_g is a function of Re_τ (see Section 5.1 for details); z is the distance from the wall and $z^+ = zu_\tau/\nu_{\text{kin}}$ is the normalised distance from the wall. Note that $z/\delta = z^+/Re_\tau$.

We use an equation for the square of the normalised fluctuating velocity u including the viscous term V as formulated in [12]:

$$\frac{\overline{u^2_{\text{g,fluc}}}(z)}{u_\tau^2} = B_{\text{g,fluc}} - A_{\text{g,fluc}}\log(z/\delta) + V(z^+) \tag{3}$$

$$= B_{\text{g,fluc}} - A_{\text{g,fluc}}\log(z/\delta) - C_{\text{g,fluc}}(z^+)^{-1/2} \tag{4}$$

$$= B_{\text{g,fluc}} - A_{\text{g,fluc}}\log(z/\delta) - \frac{C_{\text{g,fluc}}}{\sqrt{Re_\tau}}\sqrt{\frac{\delta}{z}}, \tag{5}$$

where the subscript "fluc" indicates "fluctuating". Overbar is time averaging; $A_{\mathrm{g,fluc}}$, $B_{\mathrm{g,fluc}}$ and $C_{\mathrm{g,fluc}}$ are functions of Re_τ [5], see Figure 1. Note that we show $C_{\mathrm{g,fluc}}/\sqrt{Re_\tau}$ instead of $C_{\mathrm{g,fluc}}$. These functions are assumed to be identical for smooth and rough pipe flow.

For all figures including results from the model developed in this paper, we include both smooth and rough pipe plots. For many cases, these will be identical, but for several important quantities they will differ. To make it absolutely clear to the reader when wall roughness impacts the model, we have chosen to include both plots throughout. Details on the smooth and rough pipe settings are provided in Section 7.

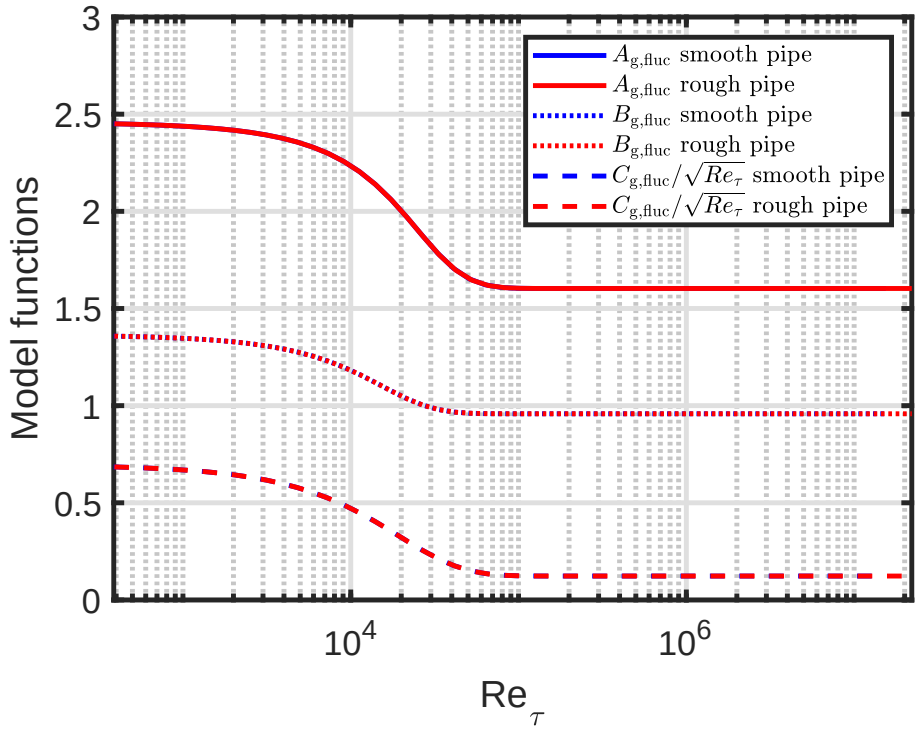

Figure 1: Functions for the square of the normalised fluctuating velocity as a function of friction Reynolds number. The smooth and rough pipe lines are identical and cannot be distinguished.

As discussed in [5], we combine our results with findings from [13] to derive an area-averaged (AA) turbulence production-to-dissipation ratio:

$$\left\langle \frac{\mathcal{P}}{\varepsilon} \right\rangle_{\mathrm{AA}} = \exp(1.49 - B_{\mathrm{g,fluc}}/0.91), \tag{6}$$

with asymptotic limits:

$$\lim_{Re_\tau \to 0} \left\langle \frac{\mathcal{P}}{\varepsilon} \right\rangle_{\mathrm{AA}} = 0.99 \tag{7}$$

$$\lim_{Re_\tau \to \infty} \left\langle \frac{\mathcal{P}}{\varepsilon} \right\rangle_{\mathrm{AA}} = 1.55, \tag{8}$$

see Figure 2. The AA definition can be found in Section 5.4.

If turbulence production matches dissipation, the flow is said to be in (local) equilibrium. This assumption is usually made for standard turbulent (eddy) viscosity models. As can be seen in Figure 2, the AA production-to-dissipation ratio is close to one for low Reynolds numbers, which can be considered as flow in (global) equilibrium. However, as the Reynolds number increases, the turbulence production becomes much larger than the turbulence dissipation, which means that the flow will not be in equilibrium. This leads to a need for an investigation on how non-equilibrium flows can be included in turbulence models. A first step in this direction - an algebraic turbulence model - is the main topic of this paper.

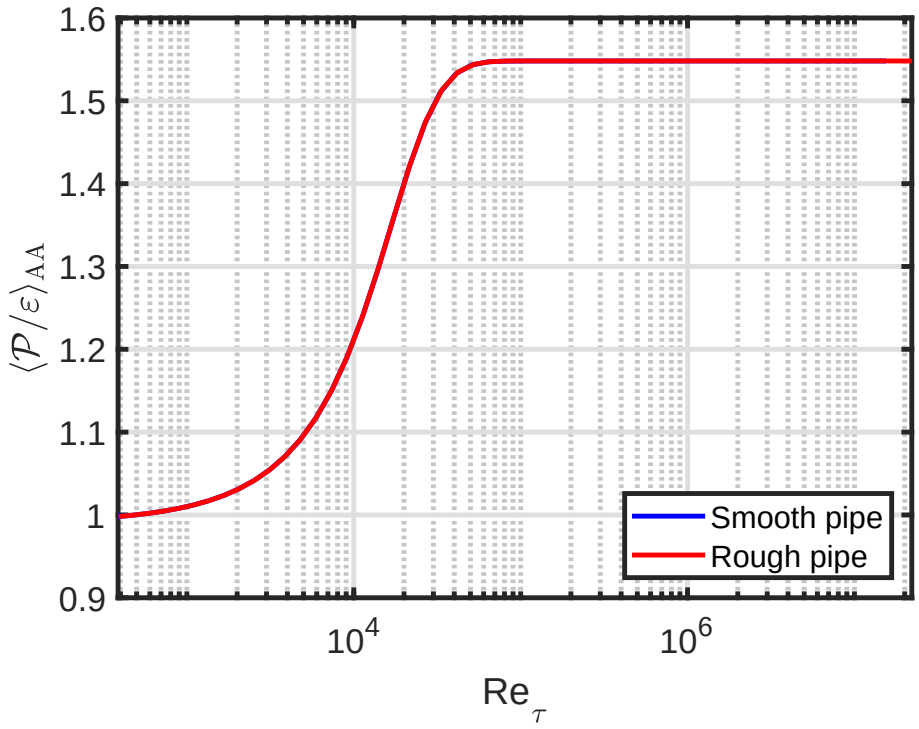

Figure 2: Area-averaged (AA) turbulence production-to-dissipation ratio as a function of friction Reynolds number. The smooth and rough pipe lines are identical and cannot be distinguished.

In the remainder of the paper, we will primarily use the expressions for the fluctuating part of the velocity; therefore we drop the subscript "fluc"; however, the subscript "mean" will be used when we are treating the mean velocity.

3. Basic model

We follow the treatment and nomenclature in [14], along with inspiration from [15].

For simplicity of exposition we treat simple shear flow, where the turbulent (eddy) viscosity (ν_t) hypothesis [16] can be written:

$$-\overline{uv} = \nu_t \times \mathcal{S}, \tag{9}$$

with $-\overline{uv}$ being the Reynolds (shear) stress of the streamwise fluctuating velocity u and the wall-normal fluctuating velocity v. The mean shear rate (mean velocity gradient) is given by:

$$\mathcal{S} = \partial U/\partial z, \tag{10}$$

which can be inverted to define a mean shear time scale:

$$\tau_{\mathcal{S}} = \frac{1}{\mathcal{S}} \tag{11}$$

The turbulence production rate is:

$$\mathcal{P} = -\overline{uv} \times \mathcal{S} = \nu_t \times \mathcal{S}^2, \tag{12}$$

where the turbulent viscosity is modelled as a product of characteristic length and velocity scales:

$$\nu_t = \ell^* \times u^* \tag{13}$$

As a characteristic length scale we use the mixing length ℓ_m which will be defined in more detail in Section 5:

$$\ell^* = \ell_m \tag{14}$$

Regarding the characteristic velocity scale, we treat the one originally proposed in Section 3.1 for reference. In the remainder of the paper we will use the modified characteristic velocity scale introduced in Section 3.2.

3.1. Original u^*

The characteristic velocity for the original mixing length hypothesis [6, 7] is:

$$u^* = u_{\mathrm{P}} = \ell_m |\mathcal{S}|, \tag{15}$$

where we use the subscript "P" for Prandtl. This characteristic velocity and Equations (13) and (14) lead to a turbulent viscosity of:

$$\nu_t = \nu_{t,\mathrm{P}} = \ell_m \times \ell_m |\mathcal{S}| = \ell_m^2 |\mathcal{S}|, \tag{16}$$

and, finally, by use of Equation (9), an expression for the Reynolds stress:

$$-\overline{uv} = -\overline{uv}_{\mathrm{P}} = \nu_t \times \mathcal{S} = \ell_m^2 \mathcal{S}|\mathcal{S}| \tag{17}$$

3.2. Modified u^*

Kolmogorov [17] and Prandtl [18] independently proposed the Kolmogorov-Prandtl velocity scale:

$$u^* = u_{\mathrm{K-P}} = c\sqrt{k}, \tag{18}$$

where the subscript "K-P" is for Kolmogorov-Prandtl, c is a constant (but turns out to be a variable for our model) to be determined and k is the turbulent kinetic energy (TKE). Now, we define the turbulent viscosity as the product of the mixing length and the Kolmogorov-Prandtl velocity scale:

$$\nu_t = \nu_{t,\mathrm{K-P}} = \ell_m \times c\sqrt{k} \tag{19}$$

Taylor proposed [19, 20] that the dissipation rate ε of the TKE can be written in this form:

$$\varepsilon = \frac{u^{*3}}{\ell^*}, \tag{20}$$

and combining this expression with Equations (14) and (18) we arrive at:

$$\varepsilon = \frac{(c\sqrt{k})^3}{\ell_m} = \frac{C_D k^{3/2}}{\ell_m}, \tag{21}$$

where $C_D = c^3$ and using Equations (19) and (21) the turbulent viscosity becomes:

$$\nu_t = cC_D \times \frac{k^2}{\varepsilon} = C_\mu \times \frac{k^2}{\varepsilon}, \tag{22}$$

with $C_\mu = c^4$. Now we are able to introduce an expression for the turbulent production-to-dissipation ratio based on Equations (12) and (21):

$$\frac{\mathcal{P}}{\varepsilon} = \frac{\ell_m^2 \times c\sqrt{k} \times \mathcal{S}^2}{C_D k^{3/2}} = \frac{\ell_m^2 \times \mathcal{S}^2}{c^2 k}, \tag{23}$$

which can be rearranged to:

$$c\sqrt{k} = \ell_m |\mathcal{S}| \left(\frac{\mathcal{P}}{\varepsilon}\right)^{-1/2} \tag{24}$$

Comparing the equations in Section 3.1 with the equations in this section, we can write the Kolgomorov-Prandtl expressions as the Prandtl equations divided by $\sqrt{\mathcal{P}/\varepsilon}$:

$$u_{\mathrm{K-P}} = \ell_m |\mathcal{S}| \left(\frac{\mathcal{P}}{\varepsilon}\right)^{-1/2} = u_{\mathrm{P}} \left(\frac{\mathcal{P}}{\varepsilon}\right)^{-1/2} \tag{25}$$

$$\nu_{t,\mathrm{K-P}} = \ell_m^2 |\mathcal{S}| \left(\frac{\mathcal{P}}{\varepsilon}\right)^{-1/2} = \nu_{t,\mathrm{P}} \left(\frac{\mathcal{P}}{\varepsilon}\right)^{-1/2} \tag{26}$$

$$-\overline{uv} = -\overline{uv}_{\mathrm{K-P}} = \ell_m^2 \mathcal{S}|\mathcal{S}| \left(\frac{\mathcal{P}}{\varepsilon}\right)^{-1/2} = -\overline{uv}_{\mathrm{P}} \left(\frac{\mathcal{P}}{\varepsilon}\right)^{-1/2} \tag{27}$$

So a production-to-dissipation ratio above one implies lower velocity, turbulent viscosity and Reynolds stress compared to the original Prandtl formulation.

3.3. Derived quantities

Manipulating the equations in Section 3.2, we can reformulate the expressions to establish alternative dependencies explicitly.

The TKE production rate can be written using Equations (21), (23) and (24):

$$\mathcal{P} = \ell_m^2 |\mathcal{S}|^3 \left(\frac{\mathcal{P}}{\varepsilon}\right)^{-1/2}, \tag{28}$$

while c, C_D and C_μ can be expressed in terms of the TKE, the mixing length, the mean shear rate and the TKE production-to-dissipation ratio using Equation (24):

$$c = \frac{\ell_m |\mathcal{S}|}{\sqrt{k}} \left(\frac{\mathcal{P}}{\varepsilon}\right)^{-1/2} \tag{29}$$

$$C_D = c^3 = \frac{\ell_m^3 |\mathcal{S}|^3}{k^{3/2}} \left(\frac{\mathcal{P}}{\varepsilon}\right)^{-3/2} \tag{30}$$

$$C_\mu = c^4 = \frac{\ell_m^4 \mathcal{S}^4}{k^2} \left(\frac{\mathcal{P}}{\varepsilon}\right)^{-2} \tag{31}$$

The TKE can be written explicitly from Equation (24)

$$k = \frac{\ell_m^2 \mathcal{S}^2}{c^2} \left(\frac{\mathcal{P}}{\varepsilon}\right)^{-1}, \tag{32}$$

and the TKE dissipation rate from Equations (21) and (24):

$$\varepsilon = \ell_m^2 |\mathcal{S}|^3 \left(\frac{\mathcal{P}}{\varepsilon}\right)^{-3/2} \tag{33}$$

The ratio of the absolute value of the Reynolds stress to the TKE can be written using Equation (27) as:

$$\frac{|\overline{uv}|}{k} = \frac{\ell_m^2 \mathcal{S}^2}{k} \left(\frac{\mathcal{P}}{\varepsilon}\right)^{-1/2}, \tag{34}$$

or - using Equations (9) and (22) - as:

$$\frac{|\overline{uv}|}{k} = \frac{\nu_t \mathcal{S}}{k} = \frac{\mathcal{S}}{k} C_\mu \frac{k^2}{\varepsilon} = C_\mu \frac{\mathcal{S}k}{\varepsilon} \tag{35}$$

The TKE production-to-dissipation ratio can be derived from Equations (12) and (22):

$$\frac{\mathcal{P}}{\varepsilon} = \frac{\nu_t \mathcal{S}^2}{\varepsilon} = \frac{\mathcal{S}^2}{\varepsilon} C_\mu \frac{k^2}{\varepsilon} = C_\mu \left(\frac{\mathcal{S}k}{\varepsilon} \right)^2 \tag{36}$$

Combining Equations (35) and (36) we can also write the ratio of the absolute value of the Reynolds stress to the TKE as:

$$\frac{|\overline{uv}|}{k} = \left(C_\mu \frac{\mathcal{P}}{\varepsilon} \right)^{1/2} \tag{37}$$

This last equation could also have been derived from Equations (31) and (34).

3.4. General formulation

Several quantities can be derived from k and ε and most will be used later in the paper. The first is a length scale where we use Equation (21):

$$L = \frac{k^{3/2}}{\varepsilon} = \frac{\ell_m}{C_D}, \tag{38}$$

and the corresponding ratio between the mixing length and this new length scale can be found using C_μ from Equation (31):

$$\frac{\ell_m}{L} = c^3 = C_\mu^{3/4} = \frac{\ell_m^3 |\mathcal{S}|^3}{k^{3/2}} \left(\frac{\mathcal{P}}{\varepsilon} \right)^{-3/2} \tag{39}$$

The second quantity is a turbulent time scale where we use Equations (21) and (35):

$$\tau_L = \frac{k}{\varepsilon} = \frac{|\overline{uv}|}{k} \frac{1}{C_\mu \mathcal{S}} = \frac{\ell_m}{C_D \sqrt{k}} = \frac{L}{\sqrt{k}} \tag{40}$$

Note that in conjunction with Equation (11), this time scale can be used to express a turbulence-to-mean shear time scale ratio:

$$\frac{\mathcal{S}k}{\varepsilon} = \frac{\tau_L}{\tau_{\mathcal{S}}} \tag{41}$$

A frequency scale can be defined as a third quantity which is the inverse of the turbulent time scale:

$$\omega_L = \frac{\varepsilon}{k} = \frac{k}{|\overline{uv}|} C_\mu \mathcal{S} = \frac{C_D\sqrt{k}}{\ell_m} = \frac{\sqrt{k}}{L} \tag{42}$$

Two-equation turbulence models can for example solve equations for k and ε ($k-\varepsilon$ [21]) or k and ω_L ($k-\omega_L$ [20]). We will return to the $k-\varepsilon$ model in Section 8.5.

As the final, fourth, quantity we define the turbulent viscosity scale based on the length scale L:

$$\nu_{t,L} = \frac{k^2}{\varepsilon} = \frac{|\overline{uv}|}{C_\mu \mathcal{S}} = \frac{\ell_m\sqrt{k}}{C_D} = \sqrt{k}L \tag{43}$$

3.5. Standard turbulence model constant C_μ

For standard turbulent viscosity models, [22] is used for the ratio of the absolute value of the Reynolds stress to the TKE:

$$\frac{|\overline{uv}|}{k} \approx 0.3 \tag{44}$$

Along with an assumption of equilibrium flow:

$$\mathcal{P} \approx \varepsilon, \tag{45}$$

we can use Equation (37) to derive the standard turbulence model constant C_μ:

$$C_{\mu,\mathrm{B}} = (0.3)^2 = 0.09, \tag{46}$$

where we use the subscript "B" for Bradshaw et al. [22].

As we have seen in Section 3.3 (Equation (31)), we predict that C_μ scales with $(\mathcal{P}/\varepsilon)^{-2}$ for non-equilibrium flows.

We note that with the assumptions above, the turbulence-to-mean shear time scale ratio is:

$$\frac{\tau_L}{\tau_\mathcal{S}} = \frac{\mathcal{S}k}{\varepsilon} = \frac{|\overline{uv}|}{k}\frac{1}{C_\mu} = \frac{10}{3}, \tag{47}$$

where we have used Equations (35) and (41).

4. Turbulent Viscosity Ratio

We define the total viscosity as the sum of the kinematic (physical property) and turbulent (flow property) viscosity:

$$\nu_{\text{tot}} = \nu_{\text{kin}} + \nu_t \tag{48}$$

From the two parts of the total viscosity we can calculate the turbulent viscosity ratio:

$$\nu_r = \frac{\nu_t}{\nu_{\text{kin}}}, \tag{49}$$

which is a quantity often used for inlet boundary conditions in CFD simulations, a typical default value being 10 [23].

The turbulence Reynolds number [14] is given as:

$$Re_L = \frac{\sqrt{k}L}{\nu_{\text{kin}}} = \frac{k^2}{\varepsilon\nu_{\text{kin}}}, \tag{50}$$

where we have used Equation (43). This means that the turbulent viscosity ratio can be written as the following product:

$$\nu_r = \frac{C_\mu \times \frac{k^2}{\varepsilon}}{\nu_{\text{kin}}} = C_\mu \times Re_L \tag{51}$$

5. Turbulent Mixing Length Scales

5.1. von Kármán number

Before explicitly documenting the mixing length scales considered, we take a look at the variation of the global von Kármán number, which is derived by assuming that the streamwise mean velocity is given by Equation (2) across the entire flow. For the Superpipe measurements, a solution to this equation is given as "Solution 2" (see [4] for details) for smooth and rough wall pipe flow in Figure 3. In [4], we used a power-law fit to the smooth pipe data, but here we show that the measurements can equally well be described by a hyperbolic tangent function:

$$\kappa_g(Re_\tau) = -1.18 + 1.52 \times \tanh(2.15 \times 10^{-4} \times (Re_\tau + 8785.94)), \tag{52}$$

with asymptotic limits:

$$\lim_{Re_\tau \to 0} \kappa_g(Re_\tau) = 0.27 \tag{53}$$

$$\lim_{Re_\tau \to \infty} \kappa_g(Re_\tau) = 0.34, \tag{54}$$

where the upper limit is close to 1/3 as advocated for in [24]. We expect that the rough wall κ_g should be identical to the smooth wall value, since roughness shifts the velocity profile without changing the slope. For the limited amount of rough wall points, it is difficult to discern if that is indeed the case.

The transition of κ_g at $Re_\tau \sim 10^4$ is consistent with the high Reynolds number transition region found previously [4, 5].

5.2. Local mixing lengths

The classical mixing length is derived from measurements in [25]:

$$\ell_{m,\mathrm{N}} = \delta \times \left[0.14 - 0.08\left(1 - \frac{z}{\delta}\right)^2 - 0.06\left(1 - \frac{z}{\delta}\right)^4\right] \tag{55}$$

$$= \delta \times \left[0.4\left(\frac{z}{\delta}\right) - 0.44\left(\frac{z}{\delta}\right)^2 + 0.24\left(\frac{z}{\delta}\right)^3 - 0.06\left(\frac{z}{\delta}\right)^4\right], \tag{56}$$

where we use the subscript "N" for Nikuradse.

Another mixing length can be derived from the log-law in Equation (2) [11]:

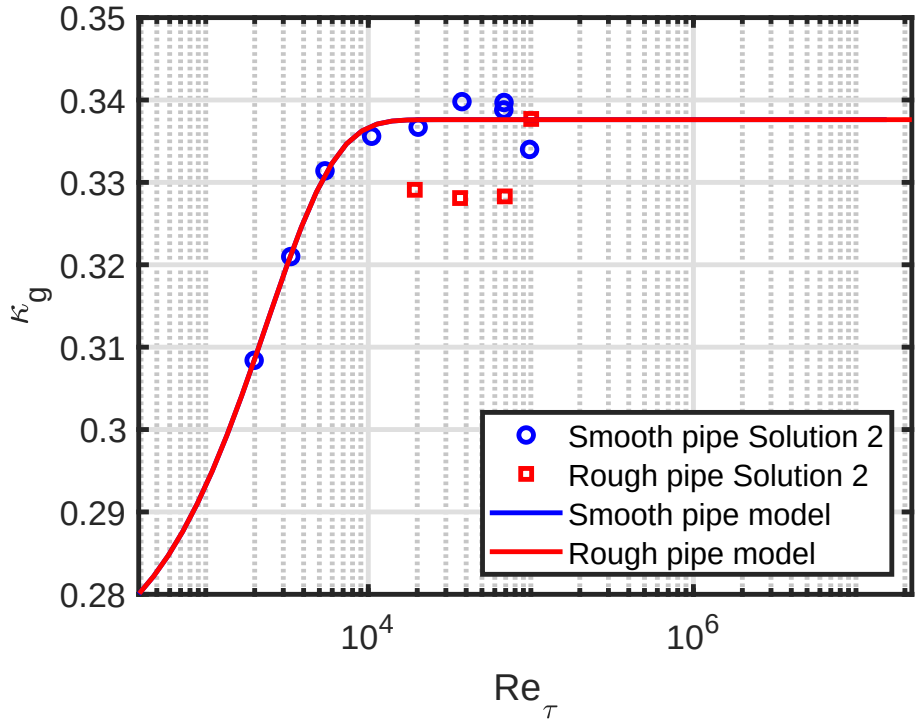

Figure 3: κ_g as a function of Re_τ. The models display Equation (52). The smooth and rough pipe lines are identical and cannot be distinguished.

$$\ell_{m,\mathrm{vK}} = \kappa_g \times z, \tag{57}$$

where we use the subscript "vK" for von Kármán. This expression implies that the mixing length increases linearly from the wall with a slope κ_g.

Finally, a third mixing length is [26]:

$$\ell_{m,\mathrm{G-H}} = \delta \times \frac{\kappa_g}{6}\left[1-\left(1-\frac{z}{\delta}\right)^2\right]\left[1+2\left(1-\frac{z}{\delta}\right)^2\right] \tag{58}$$

$$= \delta \times \kappa_g\left[\left(\frac{z}{\delta}\right)-\frac{11}{6}\left(\frac{z}{\delta}\right)^2+\frac{4}{3}\left(\frac{z}{\delta}\right)^3-\frac{2}{6}\left(\frac{z}{\delta}\right)^4\right], \tag{59}$$

where we use the subscript "G-H" for Gersten-Herwig. All three normalised mixing length expressions are compared in Figure 4; since the von Kármán and Gersten-Herwig expressions are functions of κ_g, they vary (increase) with the friction Reynolds number, whereas the Nikuradse expression is independent of Re_τ.

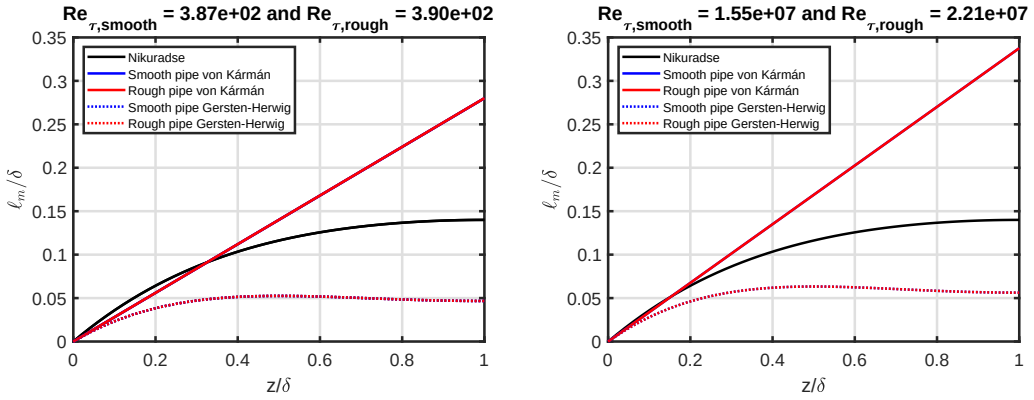

Figure 4: Normalised mixing length as a function of normalised pipe radius, left: Low friction Reynolds number, right: High friction Reynolds number. Smooth and rough pipe lines are almost identical and cannot be distinguished.

5.3. Centerline mixing lengths

The centerline (CL) value of the mixing length is the value on the pipe axis ($z/\delta = 1$). For the three mixing lengths considered, the CL values are:

$$\ell_{m,\mathrm{N,CL}} = 0.14 \times \delta \tag{60}$$

$$\ell_{m,\mathrm{vK,CL}} = \kappa_g \times \delta \tag{61}$$

$$\ell_{m,\mathrm{G-H,CL}} = \frac{\kappa_g}{6} \times \delta \tag{62}$$

5.4. Area-averaged mixing lengths

The area-average (AA) of a quantity is defined as:

$$\langle \cdot \rangle_{\mathrm{AA}} = \frac{2}{\delta^2} \int_0^{\delta} [\cdot] \times (\delta - z) \mathrm{d}z \tag{63}$$

$$= \frac{2}{Re_\tau} \int_0^{Re_\tau} [\cdot] \mathrm{d}z^+ - \frac{2}{Re_\tau^2} \int_0^{Re_\tau} [\cdot] \times z^+ \mathrm{d}z^+ \tag{64}$$

Using this averaging on our three mixing lengths in Equations (55), (57) and (58), we can write:

$$\langle \ell_{m,\mathrm{N}} \rangle_{\mathrm{AA}} = 0.08 \times \delta [27] \tag{65}$$

$$\langle \ell_{m,\mathrm{vK}} \rangle_{\mathrm{AA}} = \frac{\kappa_g}{3} \times \delta [4] \tag{66}$$

$$\langle \ell_{m,\mathrm{G-H}} \rangle_{\mathrm{AA}} = 0.14 \kappa_g \times \delta \tag{67}$$

In Figure 5, we compare the three AA normalised mixing lengths as a function of Re_τ. As mentioned earlier, the Nikuradse mixing length is independent of Re_τ, whereas the von Kármán and Gersten-Herwig mixing lengths increase across the high Reynolds number transition region due to the increase of κ_g.

The CL-to-AA mixing length ratios are all constant:

$$\frac{\ell_{m,\mathrm{N,CL}}}{\langle \ell_{m,\mathrm{N}} \rangle_{\mathrm{AA}}} = 1.75 \tag{68}$$

$$\frac{\ell_{m,\mathrm{vK,CL}}}{\langle \ell_{m,\mathrm{vK}} \rangle_{\mathrm{AA}}} = 3 \tag{69}$$

$$\frac{\ell_{m,\mathrm{G-H,CL}}}{\langle \ell_{m,\mathrm{G-H}} \rangle_{\mathrm{AA}}} = 1.19 \tag{70}$$

Using the AA formulation, we can also define the AA mean velocity as:

$$U_m = \langle U_{\mathrm{g,mean}} \rangle_{\mathrm{AA}} \tag{71}$$

6. Turbulence Intensity

6.1. Friction factor

We introduce the friction factor λ through an equation relating it to the friction velocity and the AA mean velocity:

$$u_\tau^2 = \frac{\lambda}{8} \times U_m^2, \tag{72}$$

however, we note that this equation is not completely accurate for the measurements used, see [5].

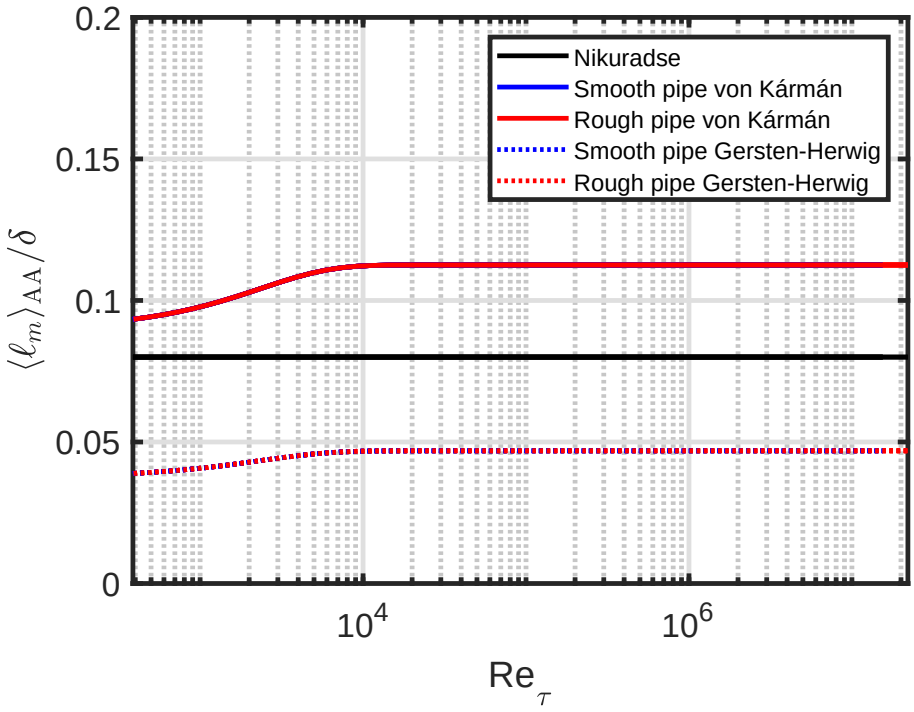

Figure 5: Area-averaged normalised mixing length as a function of the friction Reynolds number. Smooth and rough pipe lines are identical and cannot be distinguished.

6.2. TKE assumption

The TKE is equal to the sum of the contributions from streamwise, wall-normal and spanwise velocity fluctuations. We will assume that the TKE is proportional to the square of the streamwise velocity fluctuations:

$$k = \beta\overline{u^2} = \beta \times \frac{\overline{u^2}}{u_\tau^2} \times u_\tau^2 = \beta \times \frac{\overline{u^2}}{u_\tau^2} \times \frac{\lambda}{8} \times U_m^2, \tag{73}$$

where β is a constant of proportionality, see Sections 7.3 and 8.1 for more details.

6.3. Centerline

Setting $z/\delta = 1$ in Equation (3) we can write the square of the normalised CL fluctuating velocity as [28]:

$$\frac{\overline{u_{\mathrm{CL}}^2}}{u_\tau^2} = B_g - \frac{C_g}{\sqrt{Re_\tau}}, \tag{74}$$

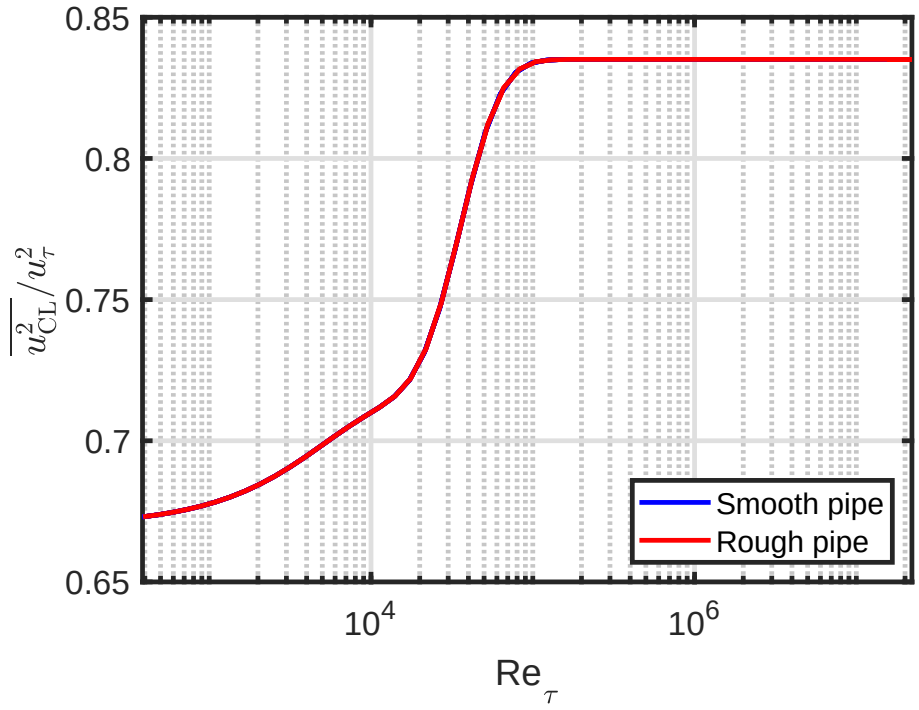

Figure 6: The square of the normalised CL fluctuating velocity as a function of Re_τ. Smooth and rough pipe lines are identical and cannot be distinguished.

which is shown in Figure 6 and observed to increase across the transition region.

The square of the turbulence intensity (TI) at the CL is defined as:

$$I_{\rm CL}^2 = \frac{\overline{u_{\rm CL}^2}}{U_{\rm CL}^2} = \frac{\overline{u_{\rm CL}^2}}{u_\tau^2} \times \frac{u_\tau^2}{U_{\rm CL}^2} \tag{75}$$

$$= \left[B_g - \frac{C_g}{\sqrt{Re_\tau}}\right] \times \frac{u_\tau^2}{U_{\rm CL}^2}, \tag{76}$$

where the mean CL velocity is related to the mean AA velocity as [29]:

$$U_{\rm CL} = 4.4441 \times u_\tau + U_m, \tag{77}$$

see Figure 7.

Finally, the CL TKE is:

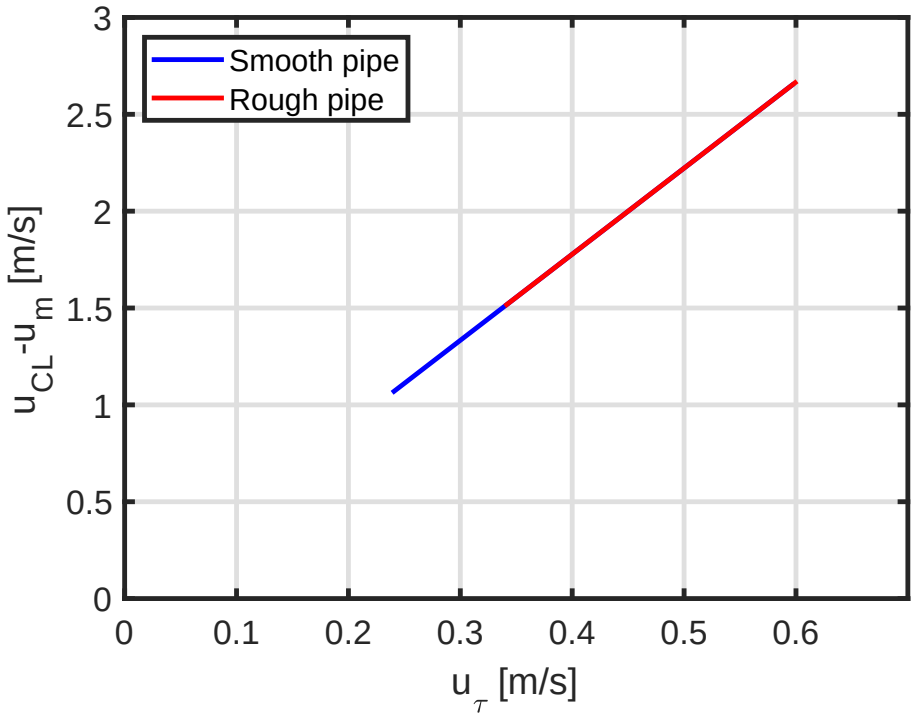

Figure 7: $U_{\mathrm{CL}} - U_m$ as a function of u_τ. Smooth and rough pipe values are on the same line.

$$k_{\mathrm{CL}} = \beta U_{\mathrm{CL}}^2 I_{\mathrm{CL}}^2 = \beta \overline{u_{\mathrm{CL}}^2} \tag{78}$$

$$= \beta \left[B_g - \frac{C_g}{\sqrt{Re_\tau}} \right] \times u_\tau^2 \tag{79}$$

6.4. Area-averaged

We repeat our CL analysis above with the AA quantities; the square of the normalised AA fluctuating velocity is [5]:

$$\frac{\langle \overline{u^2} \rangle_{\mathrm{AA}}}{u_\tau^2} = B_g + \frac{3}{2} A_g - \frac{8 C_g}{3\sqrt{Re_\tau}}, \tag{80}$$

see Figure 8. Overall the trend for higher Reynolds number is a decrease as opposed to the CL behaviour, but it has a peak value before beginning the reduction towards higher Reynolds numbers.

The square of the AA TI is defined as:

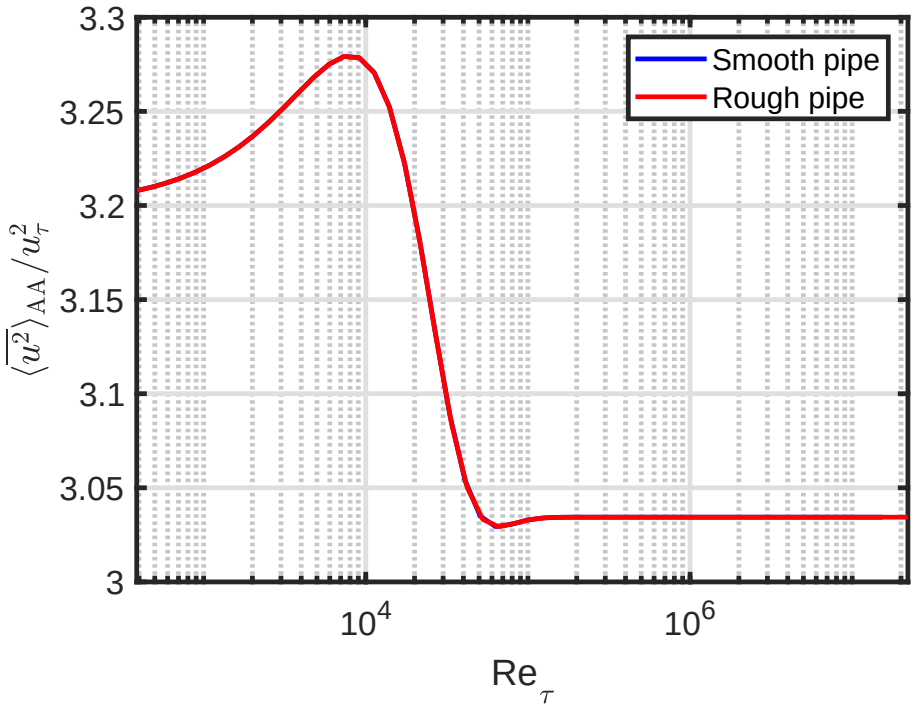

Figure 8: The square of the normalised AA fluctuating velocity as a function of Re_τ. Smooth and rough pipe lines are identical and cannot be distinguished.

$$I_{\mathrm{AA}}^2 = \frac{\overline{\langle u^2 \rangle}_{\mathrm{AA}}}{U_m^2} = \frac{\overline{\langle u^2 \rangle}_{\mathrm{AA}}}{u_\tau^2} \times \frac{u_\tau^2}{U_m^2} = \frac{\overline{\langle u^2 \rangle}_{\mathrm{AA}}}{u_\tau^2} \times \frac{\lambda}{8} \tag{81}$$

$$= \left[B_g + \frac{3}{2} A_g - \frac{8 C_g}{3\sqrt{Re_\tau}} \right] \times \frac{\lambda}{8}, \tag{82}$$

with a corresponding AA TKE:

$$k_{\mathrm{AA}} = \beta U_m^2 I_{\mathrm{AA}}^2 = \beta \overline{\langle u^2 \rangle}_{\mathrm{AA}} \tag{83}$$

$$= \beta \left[B_g + \frac{3}{2} A_g - \frac{8 C_g}{3\sqrt{Re_\tau}} \right] \times \frac{\lambda}{8} \times U_m^2 \tag{84}$$

6.5. Mixed

For reference, we include what we call the mixed TI definition from [23], which consists of a combination of CL and AA quantities [1]:

$$I_{\mathrm{mix}}^2 = \frac{\overline{u_{\mathrm{CL}}^2}}{U_m^2} = \frac{\overline{u_{\mathrm{CL}}^2}}{u_\tau^2} \times \frac{u_\tau^2}{U_m^2} = \frac{\overline{u_{\mathrm{CL}}^2}}{u_\tau^2} \times \frac{\lambda}{8} \tag{85}$$

$$= \left[B_g - \frac{C_g}{\sqrt{Re_\tau}} \right] \times \frac{\lambda}{8}, \tag{86}$$

with a corresponding mixed TKE:

$$k_{\mathrm{mix}} = \beta U_m^2 I_{\mathrm{mix}}^2 = \beta \overline{u_{\mathrm{CL}}^2} \tag{87}$$

$$= \beta \left[B_g - \frac{C_g}{\sqrt{Re_\tau}} \right] \times \frac{\lambda}{8} \times U_m^2 \tag{88}$$

7. Model results

We now apply the results from the preceding sections to the case of the Princeton Superpipe; we have calibrated the constants to this case.

7.1. Model input

The Princeton Superpipe parameters used are taken from [2]. The pipe diameters for smooth and rough pipes are:

$$D_{\mathrm{smooth}} = 2 \times 64.68 \text{ mm} \tag{89}$$

$$D_{\mathrm{rough}} = 2 \times 64.92 \text{ mm} \tag{90}$$

For the experiments, the mean velocity was held close to constant; we use this value, which is close to the ones measured:

$$U_m = 10 \text{ m/s} \tag{91}$$

The Reynolds number was mainly changed by varying the air pressure; we use a range of kinematic viscosities extending beyond the measured Reynolds numbers:

$$\nu_{\mathrm{kin}} = [10^{-9}, 10^{-4}] \text{ m}^2/\text{s} \tag{92}$$

For the rough pipe, we use the sand-grain roughness [29]:

$$k_s = 3\ \mu\text{m} \tag{93}$$

The pipe diameter, mean velocity and kinematic viscosity are used to define the bulk Reynolds number:

$$Re_D = \frac{DU_m}{\nu_{\text{kin}}} \tag{94}$$

The bulk Reynolds number and sand-grain roughness are used to derive other quantities as described in Section 7.4.

7.2. Model assumptions

For the equilibrium assumption, the Reynolds stress is related to the friction velocity as [15]:

$$-\overline{uv}_{\text{P}} = u_\tau^2 \tag{95}$$

Adapting this to non-equilibrium flows using Equation (27) we get:

$$-\overline{uv}_{\text{K}-\text{P}} = u_\tau^2 \left(\frac{\mathcal{P}}{\varepsilon}\right)^{-1/2} \tag{96}$$

Differentiating the log-law, Equation (2), with respect to z, the mean shear rate can be expressed as:

$$\mathcal{S} = \frac{u_\tau}{\ell_m}, \tag{97}$$

where ℓ_m is the von Kármán mixing length as given in Equation (57). Although inconsistent, we will assume that the mean shear rate can be expressed using the above equation even for the other two mixing lengths treated.

We will no longer assume equilibrium flows, so the two key assumptions from Section 3.5 need not be valid. Instead we explicitly write:

$$\frac{|\overline{uv}|}{k} \neq 0.3, \tag{98}$$

and:

$$\mathcal{P} \neq \varepsilon \tag{99}$$

7.3. Model choices

Since we only have the AA turbulence production-to-dissipation ratio (see Figure 2), we use AA for all other quantities as well to ensure consistency.

AA length scales can be used to define an AA mean shear rate:

$$\mathcal{S}_{\mathrm{AA}} = \frac{u_\tau}{\langle \ell_m \rangle_{\mathrm{AA}}}, \tag{100}$$

see Figure 9. We will use the Gersten-Herwig mixing length $\langle \ell_{m,\mathrm{G-H}} \rangle_{\mathrm{AA}}$, since it includes a κ_g-dependency, has been compared to measurements and possesses the correct overall behaviour of a linear rise from the wall which develops to a constant towards the CL. However, it is only roughly half of the Nikuradse length scale; it is not clear to us why there is such a large difference.

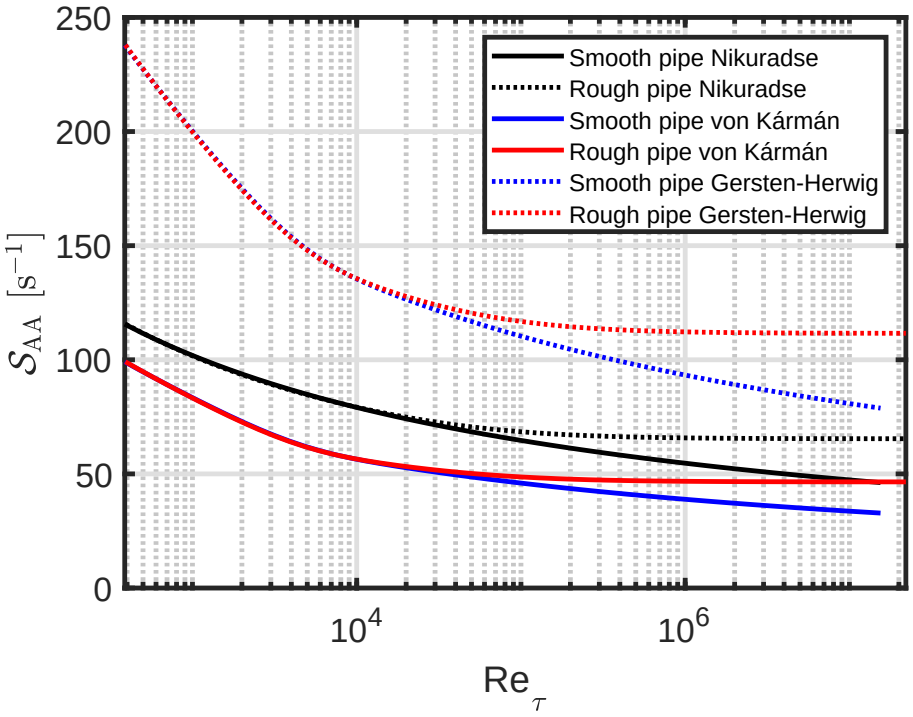

Figure 9: $\mathcal{S}_{\mathrm{AA}}$ as a function of Re_τ with length scales from Figure 5 and friction velocities from the right-hand plot in Figure 10.

We note that the log-law leads to a single length scale [4], whereas the velocity fluctuations lead to two length scales as discussed in [5].

For the TKE, $\beta = 1$ and $\beta = 1.5$ will be compared, see Section 8.1 for a discussion of those choices.

7.4. Model output

Outputs from our model will be shown for both smooth and rough pipes. The two initial quantities derived are the friction factor and the friction velocity:

1. λ from [29]
2. u_τ from Equation (72),

where the friction velocity enables the calculation of the friction Reynolds number:

$$Re_\tau = \frac{Ru_\tau}{\nu_{\text{kin}}} = \frac{u_\tau}{2U_m} \times Re_D, \tag{101}$$

see Figure 10. It is clear that the smooth and rough pipe results begin to deviate above $Re_\tau \sim 10^4$.

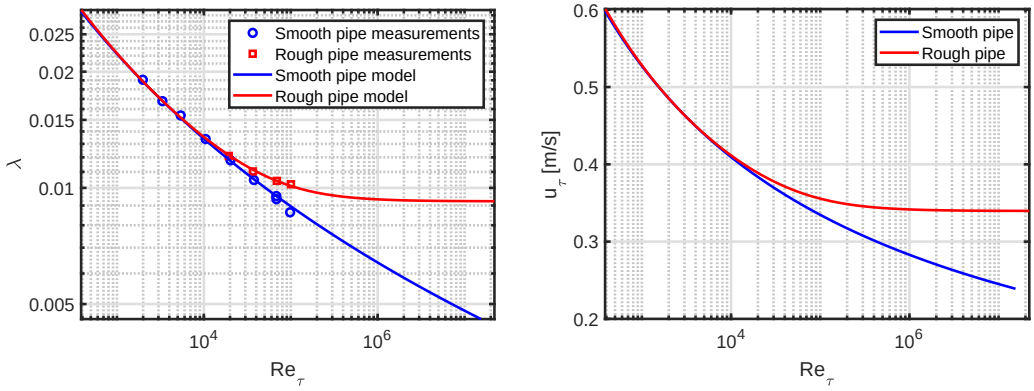

Figure 10: Left: λ as a function of Re_τ, right: u_τ as a function of Re_τ. For the friction factor, Superpipe measurements are included.

Re_τ is shown as a function of Re_D in Figure 11.

Having calculated the friction factor, we can derive the AA TI:

$$I^2_{\text{AA}} = \left[B_g + \frac{3}{2}A_g - \frac{8C_g}{3\sqrt{Re_\tau}}\right] \times \frac{\lambda}{8}, \tag{102}$$

see Figure 12. Again, the smooth and rough pipe friction factor difference is reflected in the divergence of the TI. The smooth pipe TI continues to decrease, whereas the rough pipe TI reaches a plateau.

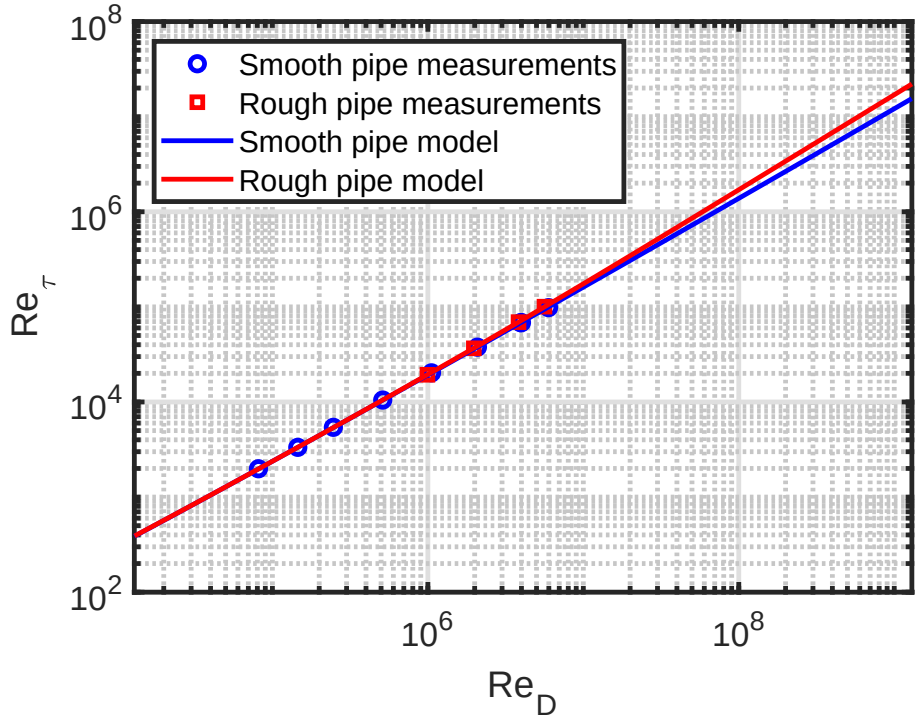

Figure 11: Friction Reynolds number as a function of bulk Reynolds number. Superpipe measurements are included.

7.4.1. Quantities depending on TKE, but not mixing length

Now we split our analysis in two parts - in this section, expressions depend on β (TKE) but not on $\langle \ell_{m,\mathrm{G-H}} \rangle_{\mathrm{AA}}$. In Section 7.4.2, we study the opposite case.

The TKE is defined as:

$$k_{\mathrm{AA}} = \beta \left[B_g + \frac{3}{2} A_g - \frac{8 C_g}{3\sqrt{Re_\tau}} \right] \times \frac{\lambda}{8} \times U_m^2, \tag{103}$$

see Figure 13. The two different β values lead to an overall shift of the TKE. The rough pipe TKE reaches a fixed value for high Reynolds numbers in contrast to the smooth pipe TKE which continues to decrease.

The ratio of the absolute value of the Reynolds stress to the TKE is:

$$\frac{|\overline{uv}|_{\mathrm{AA}}}{k_{\mathrm{AA}}} = \frac{u_\tau^2}{k_{\mathrm{AA}}} \times \left\langle \frac{\mathcal{P}}{\varepsilon} \right\rangle_{\mathrm{AA}}^{-1/2} = \frac{1}{\beta \times \left(B_g + \frac{3}{2} A_g - \frac{8 C_g}{3\sqrt{Re_\tau}} \right)} \times \left\langle \frac{\mathcal{P}}{\varepsilon} \right\rangle_{\mathrm{AA}}^{-1/2}, \tag{104}$$

which is compared to the standard value of 0.3 [22] in Figure 14. The magnitude of our AA expressions match the standard value quite well for the

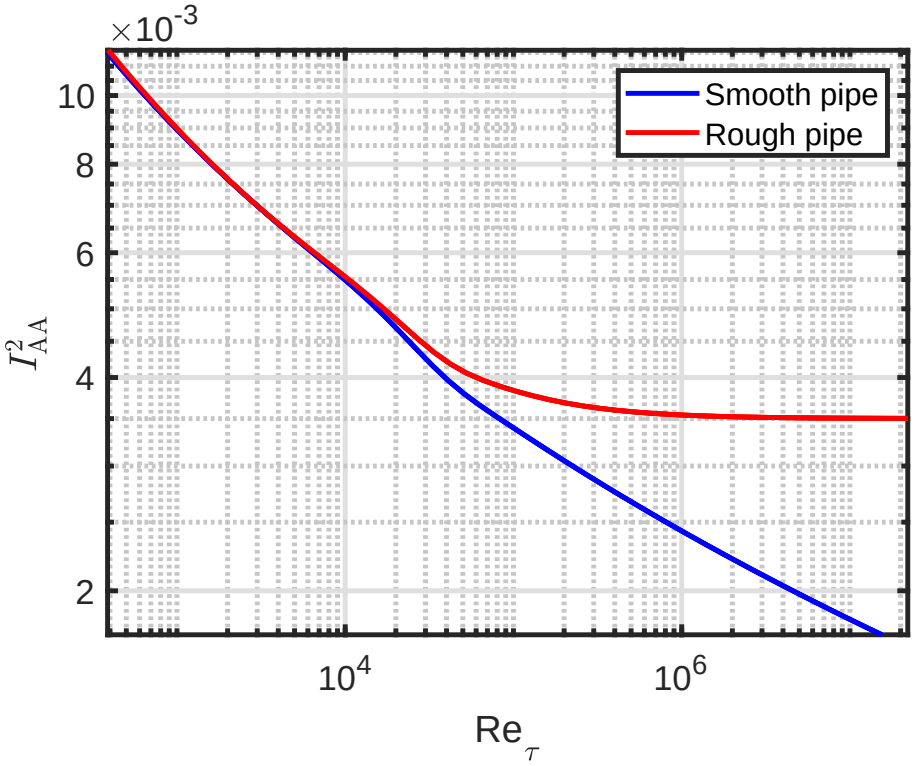

Figure 12: AA TI as a function of Re_τ.

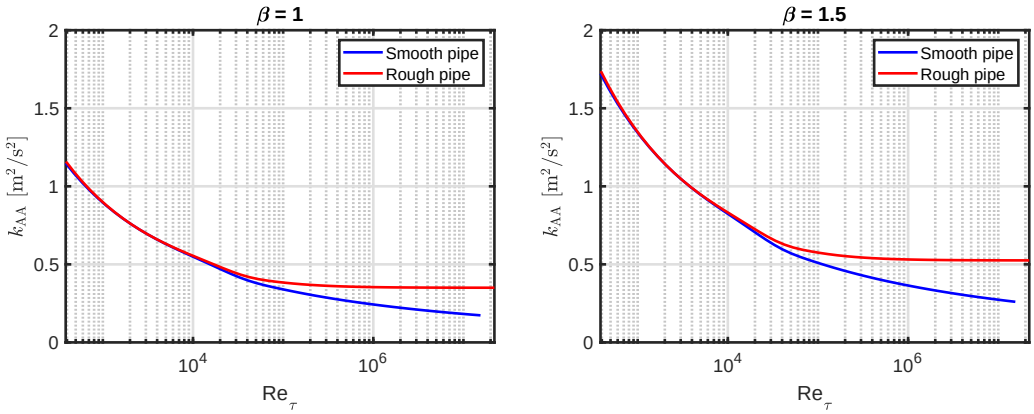

Figure 13: TKE as a function of Re_τ, left: $\beta = 1$, right: $\beta = 1.5$.

$\beta = 1$ case, but it does decrease by 15% across the high Reynolds number transition region, mainly due to the scaling with the turbulence production-to-dissipation ratio. In contrast, the magnitude of our AA expressions with $\beta = 1.5$ is much smaller than the standard value. See Section 8.3 for a discussion on these findings.

Note also that there is no difference between the smooth and rough pipe model.

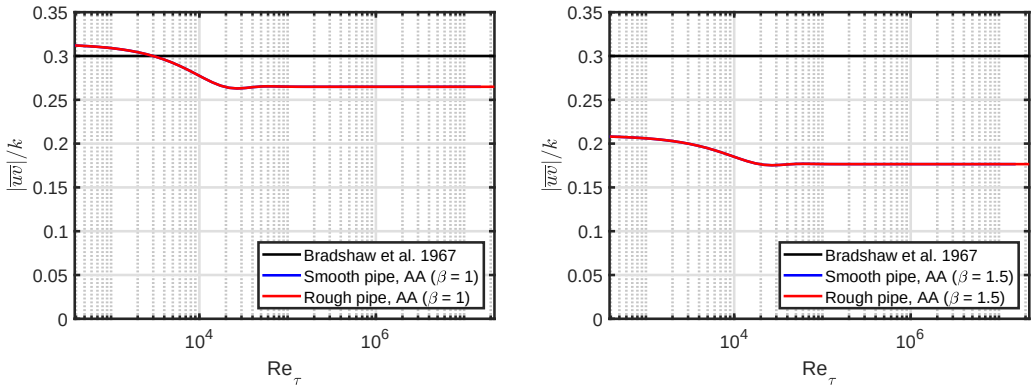

Figure 14: The ratio of the absolute value of the Reynolds stress to the TKE as a function of Re_τ, left: $\beta = 1$, right: $\beta = 1.5$. Smooth and rough pipe lines are identical and cannot be distinguished.

The AA turbulence model constant C_μ is defined as:

$$C_{\mu,\mathrm{AA}} = \frac{u_\tau^4}{k_{\mathrm{AA}}^2} \times \left\langle \frac{\mathcal{P}}{\varepsilon} \right\rangle_{\mathrm{AA}}^{-2} \tag{105}$$

$$= \frac{1}{\beta^2 \times \left(\frac{\langle \overline{u^2} \rangle_{\mathrm{AA}}}{u_\tau^2} \right)^2} \times \left\langle \frac{\mathcal{P}}{\varepsilon} \right\rangle_{\mathrm{AA}}^{-2} \tag{106}$$

$$= \frac{1}{\beta^2 \times \left(B_g + \frac{3}{2} A_g - \frac{8 C_g}{3\sqrt{Re_\tau}} \right)^2 \times \left\langle \frac{\mathcal{P}}{\varepsilon} \right\rangle_{\mathrm{AA}}^2}, \tag{107}$$

see Figure 15. For $\beta = 1$, the values at low Reynolds numbers are fairly close to the standard value of 0.09, but they decrease to around half of that value for high Reynolds numbers. An increase of β to 1.5 leads to a downward shift of C_μ. As above, we refer to Section 8.1 for a discussion of these findings.

The AA definition of the turbulence-to-mean shear time scale ratio is:

$$\left\langle \frac{\tau_L}{\tau_{\mathcal{S}}} \right\rangle_{\mathrm{AA}} = \frac{\mathcal{S}_{\mathrm{AA}} k_{\mathrm{AA}}}{\varepsilon_{\mathrm{AA}}} = \frac{\langle L \rangle_{\mathrm{AA}}}{\sqrt{k_{\mathrm{AA}}}} \frac{u_\tau}{\langle \ell_m \rangle_{\mathrm{AA}}} = \left\langle \frac{L}{\ell_m} \right\rangle_{\mathrm{AA}} \frac{u_\tau}{\sqrt{\beta \langle \overline{u^2} \rangle_{\mathrm{AA}}}}, \tag{108}$$

where we have used Equations (40) and (41), see Figure 16. The standard value of 10/3 (see Equation (47)) is included for reference. For $\beta = 1$ and low

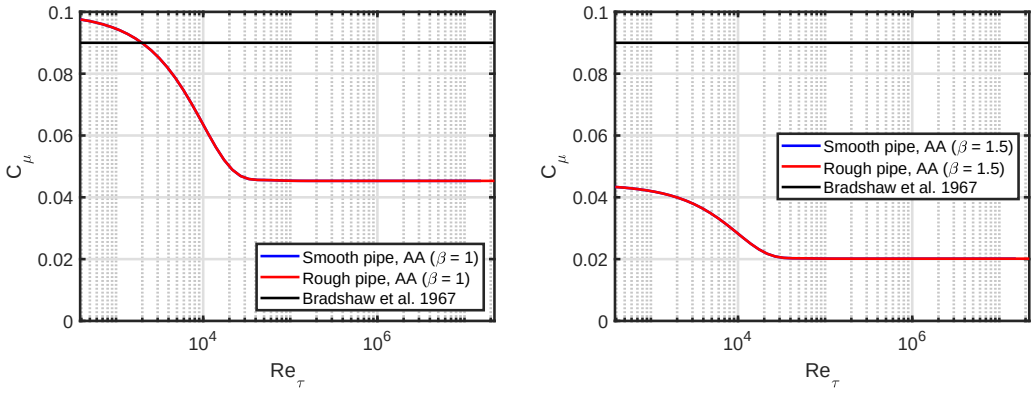

Figure 15: AA C_μ as a function of Re_τ, left: $\beta = 1$, right: $\beta = 1.5$. Smooth and rough pipe lines are identical and cannot be distinguished.

Reynolds number, the AA definition matches the standard value quite well, but increases for higher Reynolds numbers. For $\beta = 1.5$, the AA definition is shifted upwards. Other time scales are discussed in Section 8.5.

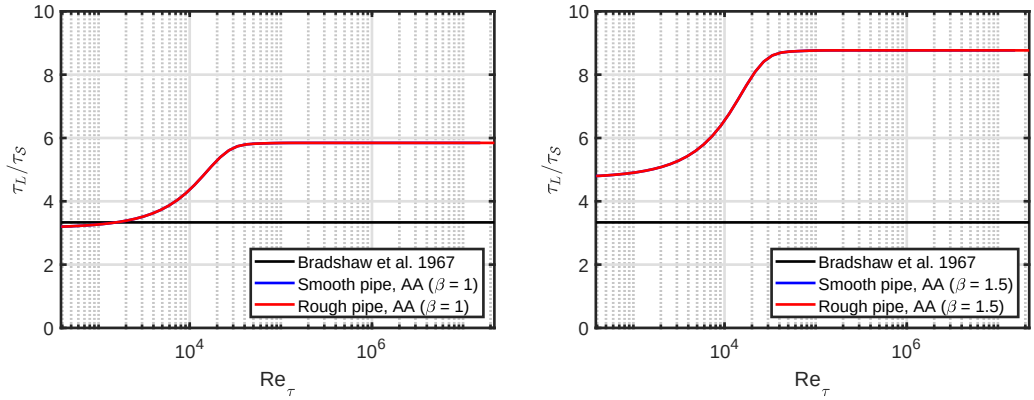

Figure 16: τ_L/τ_S as a function of Re_τ, left: $\beta = 1$, right: $\beta = 1.5$. Smooth and rough pipe lines are identical and cannot be distinguished.

Finally, we show the length scale ratio:

$$\left\langle \frac{L}{\ell_m} \right\rangle_{\mathrm{AA}} = C_{\mu,\mathrm{AA}}^{-3/4} = \beta^{3/2} \times \left(B_g + \frac{3}{2} A_g - \frac{8 C_g}{3\sqrt{Re_\tau}} \right)^{3/2} \times \left\langle \frac{\mathcal{P}}{\varepsilon} \right\rangle_{\mathrm{AA}}^{3/2}, \qquad (109)$$

see Figure 17. Overall, we conclude that $\langle L \rangle_{\mathrm{AA}} \sim 6 - 19 \times \langle \ell_m \rangle_{\mathrm{AA}}$, depending on the Reynolds number and β values. Specifically applied to the Gersten-Herwig mixing length we have:

$$\langle L_{\mathrm{G-H}} \rangle_{\mathrm{AA}} \sim 6 - 19 \times \langle \ell_{m,\mathrm{G-H}} \rangle_{\mathrm{AA}} \sim 0.3 - 1 \times \delta, \tag{110}$$

leading to an interpretation of L as being a characteristic length corresponding to the boundary layer thickness.

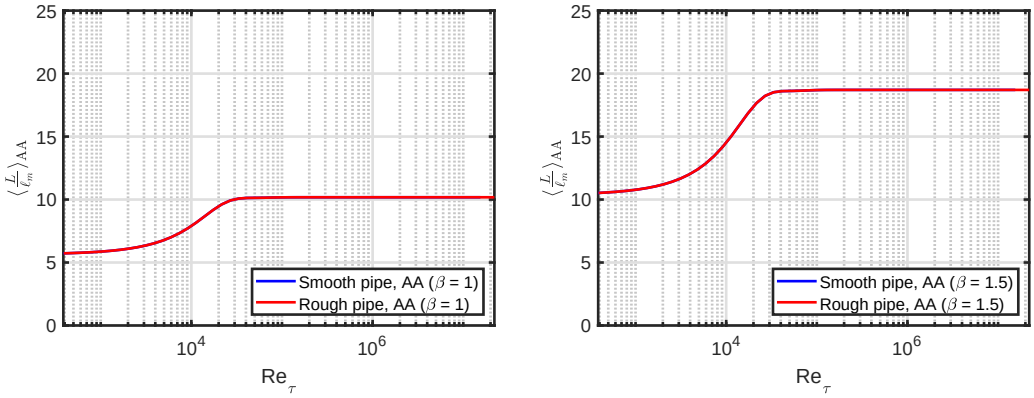

Figure 17: AA length scale ratio as a function of Re_τ, left: $\beta = 1$, right: $\beta = 1.5$. Smooth and rough pipe lines are identical and cannot be distinguished.

7.4.2. Quantities depending on mixing length, but not TKE

We now treat the inverse case of what was covered in Section 7.4.1, where the quantities depend on $\langle \ell_{m,\mathrm{G-H}} \rangle_{\mathrm{AA}}$ but not on β (TKE).

We start by writing expressions for the TKE production and dissipation rates:

$$\mathcal{P}_{\mathrm{AA}} = \frac{u_\tau^3}{\langle \ell_{m,\mathrm{G-H}} \rangle_{\mathrm{AA}}} \times \left\langle \frac{\mathcal{P}}{\varepsilon} \right\rangle_{\mathrm{AA}}^{-1/2} \tag{111}$$

$$\varepsilon_{\mathrm{AA}} = \frac{u_\tau^3}{\langle \ell_{m,\mathrm{G-H}} \rangle_{\mathrm{AA}}} \times \left\langle \frac{\mathcal{P}}{\varepsilon} \right\rangle_{\mathrm{AA}}^{-3/2} \tag{112}$$

The TKE production and dissipation rates are shown in Figure 18. The dominating quantity is u_τ^3, which leads to a rapid decrease with increasing Reynolds number. Further, the smooth pipe values continue to decrease while the rough pipe values reach a constant number.

The turbulent viscosity is given by:

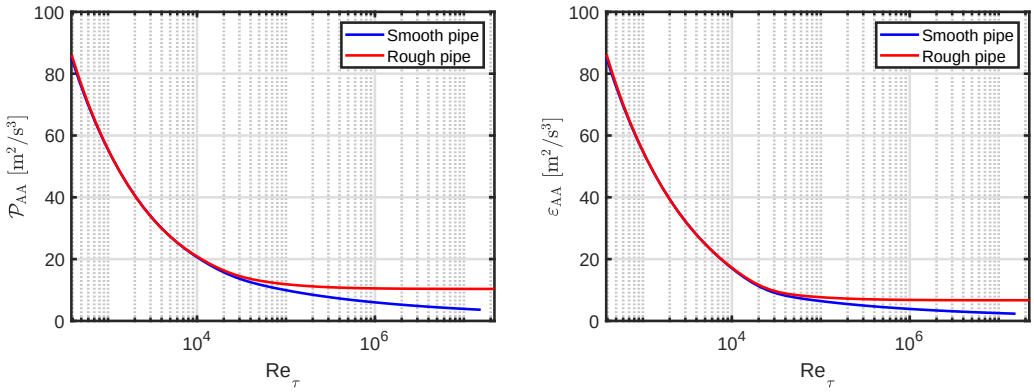

Figure 18: Left: TKE production rate as a function of Re_τ, right: TKE dissipation rate as a function of Re_τ.

$$\nu_{t,\mathrm{AA}} = u_\tau \langle \ell_{m,\mathrm{G-H}} \rangle_{\mathrm{AA}} \times \left\langle \frac{\mathcal{P}}{\varepsilon} \right\rangle_{\mathrm{AA}}^{-1/2} = C_{\mu,\mathrm{AA}} \times \frac{k_{\mathrm{AA}}^2}{\varepsilon_{\mathrm{AA}}}, \tag{113}$$

see Figure 19, with corresponding turbulent viscosity ratios in Figure 20. The values from our model do not depend on β, but for the lines marked "CL standard", there is a dependency, which will be discussed in Section 8.4.

For our model at low Reynolds numbers, the turbulent viscosity decreases for increasing Reynolds number for both smooth and rough pipes. For high Reynolds numbers, the smooth pipe turbulent viscosity continues to decrease, while the rough pipe turbulent viscosity approaches a constant value. For both smooth and rough pipes there is a transition region which is due to the combination of the Reynolds number dependency of the von Kármán number and the turbulence production-to-dissipation ratio.

The turbulent viscosity ratio covers a large range from about 10 to 10^6 which is directly linked to the range of the kinematic viscosities in Equation (92).

8. Discussion

8.1. Turbulence isotropy

β as defined in Equation (73) is 1.5 for isotropic turbulence, where each of the three fluctuating velocity components contribute equally. For actual flows, what is typically observed is that half of the TKE is in the streamwise fluctuations and the other half in the sum of the wall-normal and spanwise fluctuations, which implies a β of 1 [26, 30].

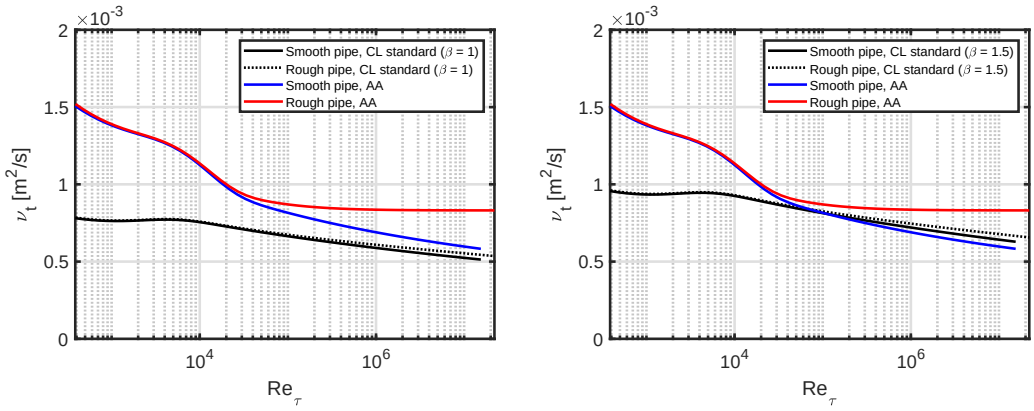

Figure 19: Turbulent viscosity as a function of Re_τ, left: $\beta = 1$, right: $\beta = 1.5$.

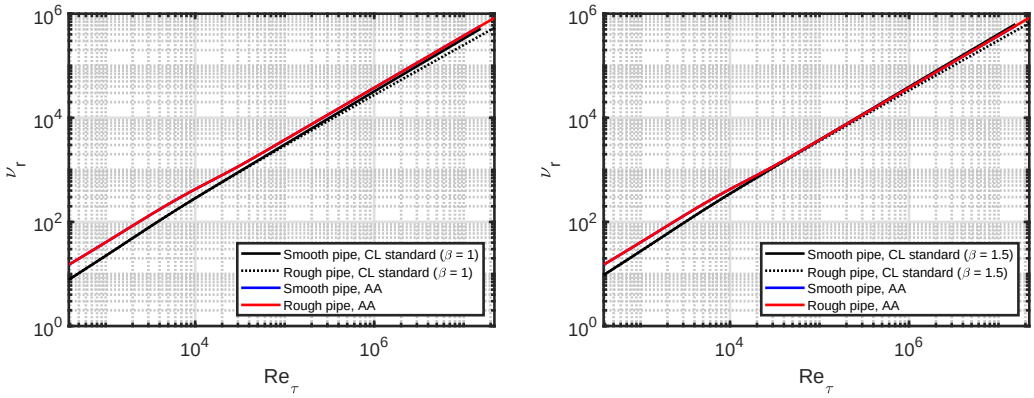

Figure 20: Turbulent viscosity ratio as a function of Re_τ, left: $\beta = 1$, right: $\beta = 1.5$.

An open question is whether β is a function of Re_τ or if variations in $\mathcal{P}/\varepsilon$ (based on streamwise fluctuations) are related to a change in β?

We will use a Reynolds number independent $\beta = 1$ for all figures in Section 8, but note that this is an assumption which can - and should - be questioned.

8.2. Physical mechanism

One explanation for the high Reynolds number transition region is an increase of large scale structures in the wake region. This can be thought of as an analogy to the "drag crisis" [31].

The question is if these structures are active or inactive, i.e. if they contribute to the turbulent shear stress or not.

In [22], the ratio of the absolute value of the Reynolds stress to the TKE is discussed: "In the last-named paper, evidence is presented that the considerable variation in a_1, observed experimentally is at least partly due to an

'inactive', quasiirrotational component of the turbulent motion (Townsend 1961), which does not contribute to the shear stress or the dissipation and can therefore be disregarded; therefore a_1 = constant is a much better approximation than at first appears." In our notation, $2a_1 = |\overline{uv}|/k$ and it is thus argued that this quantity can be considered constant.

A similar interpretation is provided in [32], which cites results from [33]: "[...]which argued that the excess of turbulent production in the log layer feeds inactive motions that do not contribute to the turbulent shear stress, but transfer energy to other locations of the flow.".

An opposing view can be found in [34], where it is stated that very-large-scale motions (VLSM) "[...]can contain up to 60% of the cumulative fraction of the Reynolds shear stress[...]".

To summarise, it remains unclear to which extent the high Reynolds number structures contribute to the turbulent shear stress.

An additional uncertainty of our analysis is that it is based on the Princeton Superpipe measurements, where it has been found that the inner peak of the streamwise fluctuations is not resolved for all Reynolds numbers [35]. However, our main results should be robust, since the global (integral) treatment is not dominated by this inner peak.

8.3. Scaling of C_μ

Scaling of C_μ with $\mathcal{P}/\varepsilon$ has been discussed in [36]. We note that the definition of $\mathcal{P}/\varepsilon$ in [36] is different from our ours; in [36], $\mathcal{P}/\varepsilon$ is weighted with $|\overline{uv}|$, whereas we use area-averaging. An expression for C_μ as a function of $\mathcal{P}/\varepsilon$, valid for $\mathcal{P}/\varepsilon > 1$, is given as:

$$C_{\mu,\mathrm{R}} = \frac{2}{3} \times \frac{1-\alpha_0}{\omega_0} \times \frac{1 - \frac{1}{\omega_0}(1 - \alpha_0 \langle \mathcal{P}/\varepsilon \rangle_{\mathrm{AA}})}{\left[1 + \frac{1}{\omega_0}(\langle \mathcal{P}/\varepsilon \rangle_{\mathrm{AA}} - 1)\right]^2}, \tag{114}$$

with:

$$\alpha_0 = 2.8 \tag{115}$$

$$\omega_0 = 0.55, \tag{116}$$

where we use the subscript "R" for Rodi and have replaced the turbulence production-to-dissipation ratio from [36] with our area-averaged definition.

As written in [36], under certain conditions "[...]the mixing length hypothesis implies that $\mathcal{P}/\varepsilon$ is constant; but $\mathcal{P}/\varepsilon$ need not equal unity.".

In Figure 21, $C_{\mu,\mathrm{R}}$ from [36] is compared to $C_{\mu,\mathrm{B}}/\langle\mathcal{P}/\varepsilon\rangle_{\mathrm{AA}}$ and our AA expressions.

The difference in scaling with $\mathcal{P}/\varepsilon$ between previous findings and our results originates from the assumption of whether $|\overline{uv}|$ scales with $\mathcal{P}/\varepsilon$ or not: Overall, previous findings predict a scaling of C_μ with $(\mathcal{P}/\varepsilon)^{-1}$, while our expressions imply a scaling of C_μ with $(\mathcal{P}/\varepsilon)^{-2}$. In [36], the weighting of $\mathcal{P}/\varepsilon$ with $|\overline{uv}|$ complicates the comparison somewhat.

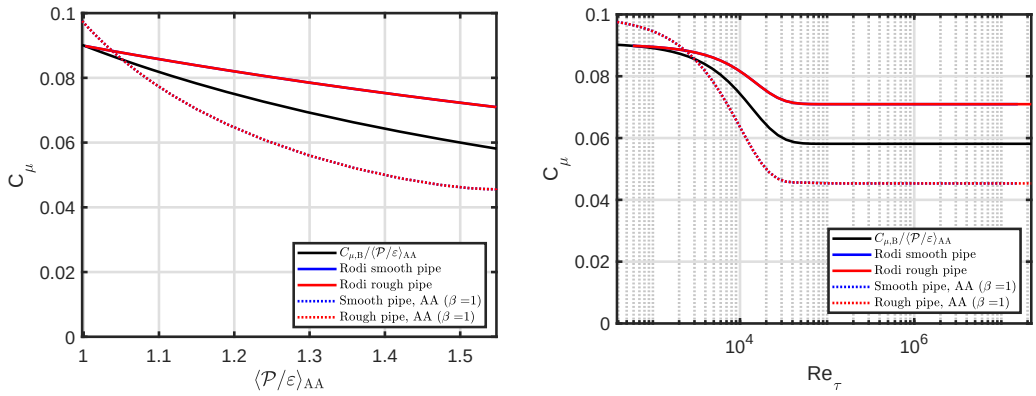

Figure 21: $C_{\mu,\mathrm{R}}$ from [36] compared to $C_{\mu,\mathrm{B}}/\langle\mathcal{P}/\varepsilon\rangle_{\mathrm{AA}}$ and our AA expressions, left: As a function of $\langle\mathcal{P}/\varepsilon\rangle_{\mathrm{AA}}$, right: As a function of Re_τ. Smooth and rough pipe lines are identical and cannot be distinguished.

8.4. Scaling of ν_t and I

The scaling of the turbulent viscosity can be compared to the standard CL expression from [9], which we have modified to include β specifically:

$$\nu_{t,\mathrm{CL}} = \sqrt{\beta} C_{\mu,\mathrm{B}}^{1/4} \times U_{\mathrm{CL}} I_{\mathrm{CL}} \ell_{m,\mathrm{G-H,CL}}, \tag{117}$$

where we use [37]:

$$I_{\mathrm{CL}} = 0.055 \times Re_D^{-0.041} \tag{118}$$

In Figures 19 and 20 we have included the turbulent viscosity from Equation (117) and marked it "CL standard". This does not match our model for the low Reynolds number range, but it does match the smooth pipe model expression quite well for the high Reynolds number range and $\beta = 1.5$. There is no β dependency of the turbulent viscosity in our model.

8.5. Time scales

From the log-law mean velocity, a single length scale is associated with the von Kármán mixing length. Or rather, a continuum of length scales increasing from the wall.

In contrast, the mixing length expressions by Nikuradse and Gersten-Herwig can be considered as consisting of two different ranges, one close to the wall and another one towards the CL. These length scales can be used to define two time scales. A similar conclusion can be drawn from the fluctuations as defined in Equation (3), which also correspond to two length scales as noted in [5].

Below, we will explore the idea of two time scales based on the assumption of two corresponding length scales. Note that a different time scale ratio for the turbulence-to-mean shear is contained in our model and has been treated in Sections 3.4 and 3.5, see also Figure 16.

8.5.1. $k-\varepsilon$ turbulence model with two time scales

Turbulence models with multiple time scales have been treated in [38], with more recent further development to be found in [39]. We base our discussion on homogeneous flow, where equations for the time evolution of k and ε can be written [40]:

$$\frac{\mathrm{d}k}{\mathrm{d}t} = \mathcal{P} - \frac{\varepsilon}{c_s} \tag{119}$$

$$\frac{\mathrm{d}\varepsilon}{\mathrm{d}t} = \left(C_{\varepsilon 1}\mathcal{P} - C_{\varepsilon 2}\frac{\varepsilon}{c_s} \right) \frac{\varepsilon}{k}, \tag{120}$$

where the standard values of the coefficients $C_{\varepsilon 1} = 1.44$, $C_{\varepsilon 2} = 1.92$ [41] and:

$$c_s = \frac{\tau_{\mathrm{fluc}}}{\tau_{\mathrm{mean}}} \tag{121}$$

is the ratio of the turbulence and the mean flow time scales. Note that $c_s = 1$ for the standard $k-\varepsilon$ model [21].

The evolution of the turbulence time scale $\tau_{\mathrm{fluc}} = \tau_L = k/\varepsilon$ (see Equation (40)) is given as [40]:

$$\frac{\mathrm{d}(k/\varepsilon)}{\mathrm{d}t} = (1 - C_{\varepsilon 1})\frac{\mathcal{P}}{\varepsilon} - \frac{1}{c_s}(1 - C_{\varepsilon 2}) \tag{122}$$

If k/ε does not vary with time, $\mathrm{d}(k/\varepsilon)/\mathrm{dt} = 0$ and we have:

$$c_s = \left(\frac{C_{\varepsilon 2} - 1}{C_{\varepsilon 1} - 1}\right)\left(\frac{\mathcal{P}}{\varepsilon}\right)^{-1}, \tag{123}$$

which can be written for AA as:

$$\langle c_s \rangle_{\mathrm{AA}} = \left(\frac{C_{\varepsilon 2} - 1}{C_{\varepsilon 1} - 1}\right)\left\langle\frac{\mathcal{P}}{\varepsilon}\right\rangle_{\mathrm{AA}}^{-1} = 2.1 \times \left\langle\frac{\mathcal{P}}{\varepsilon}\right\rangle_{\mathrm{AA}}^{-1}, \tag{124}$$

where the final equation assumes that $C_{\varepsilon 1}$ and $C_{\varepsilon 2}$ are constant, i.e. do not scale with Re_τ (or, equivalently, with $\mathcal{P}/\varepsilon$). See Figure 22, where this $k-\varepsilon$ expression is equal to the 2.1 "Standard $k-\varepsilon$" value for low Reynolds numbers and decreases monotonically to 1.4 for high Reynolds numbers.

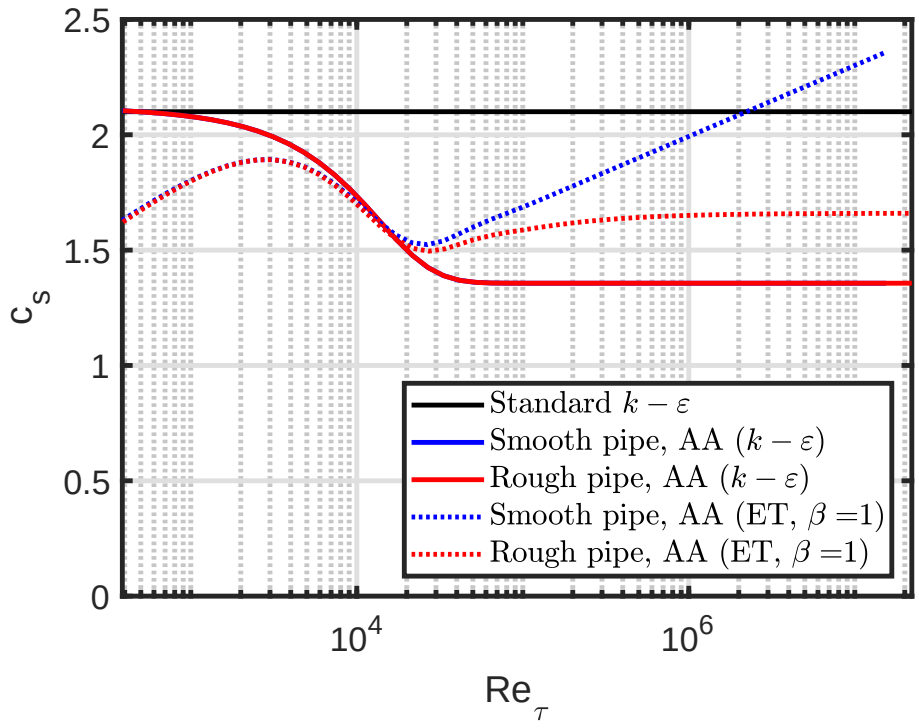

Figure 22: c_s as a function of Re_τ. The smooth and rough pipe lines (for $k-\varepsilon$) are identical and cannot be distinguished.

8.5.2. Eddy-turnover time scales

An alternative time scale ratio can be defined by an eddy-turnover (ET) time, both for the fluctuations and for the mean flow [14]:

$$\tau_{\mathrm{ET,fluc}} = \frac{\ell_m}{\sqrt{\overline{u^2}}} \tag{125}$$

$$\tau_{\mathrm{ET,mean}} = \frac{L}{U}, \tag{126}$$

along with their ratio:

$$c_{s,\mathrm{ET}} = \frac{\tau_{\mathrm{ET,fluc}}}{\tau_{\mathrm{ET,mean}}} = \frac{\ell_m}{L}\frac{U}{\sqrt{\overline{u^2}}} \tag{127}$$

For AA, this can be rewritten to:

$$\langle c_{s,\mathrm{ET}} \rangle_{\mathrm{AA}} = \left\langle \frac{\ell_m}{L} \right\rangle_{\mathrm{AA}} \times \frac{1}{\sqrt{I_{\mathrm{AA}}^2}}, \tag{128}$$

see the plots in Figure 22 marked "ET". The range of c_s values is similar to the ones from Section 8.5.1, but not monotonic. The main difference is the increase of $\langle c_{s,\mathrm{ET}} \rangle_{\mathrm{AA}}$ for the smooth pipe which is due to an increase of the fluctuating time scale, which in turn is due to a decreasing TKE.

8.5.3. Time evolution of TKE

The time scale ratio from Section 8.5.1 can be used to define an equation for the time evolution of the TKE:

$$\frac{\tau_L}{k}\frac{\mathrm{d}k}{\mathrm{d}t} = \frac{\mathcal{P}}{\varepsilon} - \frac{1}{c_s}, \tag{129}$$

which has the solution:

$$k(t) = k(0) \exp\left[\frac{t}{\tau_L}\left(\frac{\mathcal{P}}{\varepsilon} - \frac{1}{c_s}\right)\right], \tag{130}$$

where k grows if:

$$\frac{\mathcal{P}}{\varepsilon} > \frac{1}{c_s} \tag{131}$$

Defining normalised quantities $k^*(t) = k(t)/k(0)$ and $t^* = \mathcal{S}t$ [42] we can rewrite Equation (130) to:

$$k^*(t^*) = \exp\left[t^* \times \frac{1}{\tau_L \mathcal{S}}\left(\frac{\mathcal{P}}{\varepsilon} - \frac{1}{c_s}\right)\right] \tag{132}$$

$$= \exp\left[t^* \times \frac{kC_\mu}{|\overline{uv}|}\left(\frac{\mathcal{P}}{\varepsilon} - \frac{1}{c_s}\right)\right], \tag{133}$$

where we have used Equation (35) for the second equation.

For $c_s = 2.1$ and the definitions in Section 3.5, $kC_\mu/|\overline{uv}| = 0.3$ and we can add values to the equation:

$$k^*_{\mathrm{B}}(t^*) = \exp\left[0.16 \times t^*\right] \tag{134}$$

$$= \exp\left[c^*_{\mathrm{B}} \times t^*\right], \tag{135}$$

where c^*_{B} is shown in Figure 23 and k^*_{B} is shown in Figure 24.

As for the standard definitions, we can write the TKE as a function of time for our AA model with $c_{s,\mathrm{ET}}$:

$$k^*_{\mathrm{AA}}(t^*) = \exp\left[\frac{k_{\mathrm{AA}} C_{\mu,\mathrm{AA}}}{|\overline{uv}|_{\mathrm{AA}}}\left(\left\langle\frac{\mathcal{P}}{\varepsilon}\right\rangle_{\mathrm{AA}} - \frac{1}{\langle c_{s,\mathrm{ET}}\rangle_{\mathrm{AA}}}\right) \times t^*\right] \tag{136}$$

$$= \exp\left[c^*_{\mathrm{AA}} \times t^*\right], \tag{137}$$

also shown in Figures 23 (c^*_{AA}) and 24 (k^*_{AA}).

In Figure 23 we see that c^*_{AA} is a function of Reynolds number as opposed to c^*_{B} which is independent of Reynolds number. The increase of c^*_{AA} for the smooth pipe is because of an increase of $\langle c_{s,\mathrm{ET}}\rangle_{\mathrm{AA}}$. It is interesting to note that for high Reynolds numbers, k^*_{AA} increases faster for the smooth pipe than for the rough pipe.

8.6. A plasma physics analogy

An analogy for the high Reynolds number transition is a controlled confinement transition in fusion plasmas [43]. Here, a change in the topology of the magnetic field triggers a transition from "good" to "bad" confinement, where the temperature gradient decreases and the core turbulence level increases [44].

In a similar fashion, the mean velocity gradient decreases (mixing length increases) and the CL velocity fluctuations increase with increasing Reynolds number, see Figures 5 and 6.

Thus the low (high) Reynolds number range corresponds good (bad) confinement, respectively. One physical aspect which may play a part is the emergence of large structures for the pipe flow case and correlated density-magnetic fluctuations for the fusion plasma example.

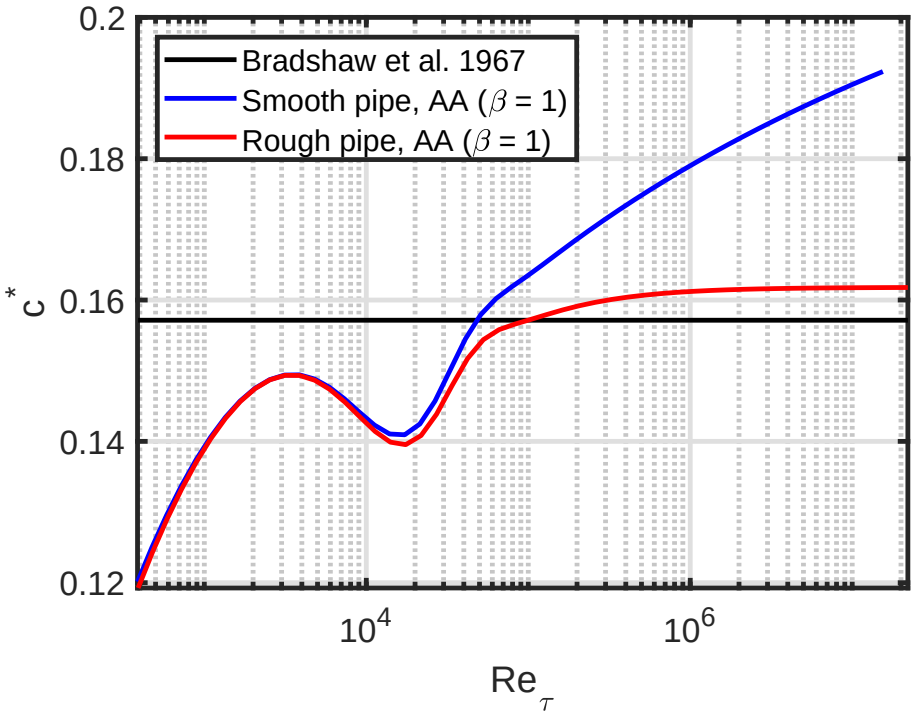

Figure 23: c^* as a function of Re_τ.

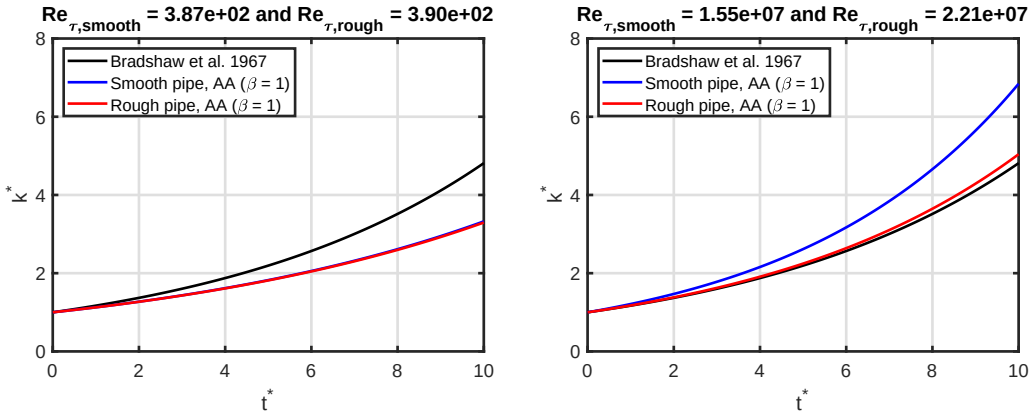

Figure 24: k^* as a function of t^*, left: Low friction Reynolds number, right: High friction Reynolds number.

8.7. Recommendations for CFD practitioners

In addition to being used for inlet boundary conditions in CFD simulations, the model output can be used as a complete, self-consistent model. These two applications are described in the following two sections.

For both applications we recommend to use $\beta = 1$ for the TKE, since this

matches the standard turbulence model for low Reynolds numbers.

8.7.1. Equilibrium usage as inlet boundary conditions for CFD simulations

The standard turbulence models in CFD simulations assume equilibrium flow; therefore we set the AA turbulence production-to-dissipation ratio equal to one. For this case, we compare the LIKE algorithm to our proposed equilibrium model in Table 1. Some comments are in order regarding the contents of the table:

- L: The expressions are taken from Equations (60) (Nikuradse) and (67) (Gersten-Herwig). Note that $\ell_{\mathrm{LIKE}}/\ell_{\mathrm{AA}} = 1/\kappa_g \sim 3$.
- I: The mix power-law expression is derived in [23] with more details provided in [1]. The equilibrium model formulation is from Equation (102).
- K: The mix and equilibrium expressions are from Equations (87) and (83).
- E: For the equilibrium model, we define $C_{\mu,\mathrm{AA}}^{3/4} = \left(B_g + \frac{3}{2}A_g - \frac{8C_g}{3\sqrt{Re_\tau}}\right)^{-3/2}$, see Equation (107). There is a difference of a factor $C_\mu^{1/4}$ between the TKE dissipation rates, which (partially) compensates for the difference between the length scales. Note that $C_{\mu,\mathrm{AA}}$ is a function of Re_τ whereas the LIKE algorithm uses the fixed standard value $C_{\mu,\mathrm{B}}$, see Section 3.5.

We are of the opinion that consistent units must be used to define all turbulent quantities, i.e. either CL or AA. The mixed TI (I_{mix}) is not straightforward to interpret and thus caution is advised for this definition.

The LIKE algorithm can be viewed as a CL model, since the used mean velocity U_m cancels out for the TKE. However, I_{mix} remains a mixture of CL and AA quantities. The LIKE algorithm could be made into a consistent CL model by replacing the existing mixed TI definition with the CL TI definition presented in Equation (75).

Thus, the AA-based equilibrium model we propose is more consistent than what is presented in the LIKE algorithm. Another advantage of the equilibrium model is that wall roughness is taken into account through the friction factor.

8.7.2. Non-equilibrium usage as a standalone model

The recommendation for use of the non-equilibrium model as a standalone model is to use the AA expressions in Section 7.4 with $\beta = 1$.

Table 1: A comparison between the LIKE algorithm [10] and the proposed equilibrium model.

Source	LIKE algorithm	Equilibrium model
L	$\ell_{\mathrm{LIKE}} = \ell_{m,\mathrm{N,CL}} = 0.14 \times \delta$	$\ell_{\mathrm{AA}} = \langle \ell_{m,\mathrm{G-H}} \rangle_{\mathrm{AA}} = 0.14\kappa_g \times \delta$
I	$I_{\mathrm{LIKE}} = I_{\mathrm{mix}} = 0.16 \times Re_D^{-1/8}$	$I_{\mathrm{AA}} = \sqrt{\left[B_g + \frac{3}{2}A_g - \frac{8C_g}{3\sqrt{Re_\tau}}\right] \times \frac{\lambda}{8}}$
K	$k_{\mathrm{LIKE}} = k_{\mathrm{mix}} = U_m^2 I_{\mathrm{mix}}^2$	$k_{\mathrm{AA}} = U_m^2 I_{\mathrm{AA}}^2$
E	$\varepsilon_{\mathrm{LIKE}} = C_{\mu,\mathrm{B}} \times \frac{k_{\mathrm{LIKE}}^{3/2}}{\ell_{\mathrm{LIKE}}}$	$\varepsilon_{\mathrm{AA}} = C_{\mu,\mathrm{AA}}^{3/4} \times \frac{k_{\mathrm{AA}}^{3/2}}{\ell_{\mathrm{AA}}} = \frac{k_{\mathrm{AA}}^{3/2}}{L_{\mathrm{AA}}}$

8.8. Known model issues

Our model is not able to capture low Reynolds number effects such as the decrease of C_μ [21, 45]. This is because the hyperbolic tangent functions used can only describe a single transition, which in our case is the high Reynolds number transition.

9. Conclusions

An algebraic mixing length non-equilibrium turbulence model has been developed to capture the high Reynolds number transition observed in pipe flow. The model equations have been derived to take the turbulence production-to-dissipation ratio explicitly into account. We provide area-averaged (integral) quantities and examples to match the Princeton Superpipe measurements used to calibrate the model, both for smooth and rough pipes.

The impact of isotropic or non-isotropic turbulence is investigated and area-averaged scaling of relevant figures-of-merit are included such as turbulent viscosity, C_μ and time scales. We expect the predictions to be valid both for pipes and similar geometries such as closed/open channel flow, see [46] and [47], respectively.

A next step could be to use a similar non-equilibrium approach for more complex one- or two-equation turbulent viscosity models.

Future research could be to generalise to rotating flows, see e.g. an extended expression for C_μ which has been proposed [48].

Acknowledgements. We thank Professor Alexander J. Smits for making the Princeton Superpipe data publicly available.

Data availability statement. Data sharing is not applicable to this article as no new data were created or analyzed in this study.

References

[1] Basse NT. Mind the gap: Boundary conditions for turbulence modelling. [Online]
`https://www.researchgate.net/publication/359218404_Mind_the_Gap_Boundary_Conditions_for_Turbulence_Modelling`
(accessed January 2023)

[2] Hultmark M, Vallikivi M, Bailey SCC and Smits AJ. Logarithmic scaling of turbulence in smooth- and rough-wall pipe flow. J. Fluid Mech. **728**, 376-395 (2013).

[3] Smits AJ. Princeton Superpipe measurements. [Online]
`https://smits.princeton.edu/superpipe-turbulence-data`
(accessed January 2023)

[4] Basse NT. Scaling of global properties of fluctuating and mean streamwise velocities in pipe flow: Characterization of a high Reynolds number transition region. Phys. Fluids **33**, 065127 (2021).

[5] Basse NT. Scaling of global properties of fluctuating streamwise velocities in pipe flow: Impact of the viscous term. Phys. Fluids **33**, 125109 (2021).

[6] Prandtl L. Bericht über Untersuchungen zur ausgebildeten Turbulenz. Z. Angew. Math. Mech. **5**, 136–139 (1925).

[7] Prandtl L. Bericht über neuere Turbulenzforschung, in: Hydraulische Probleme. *VDI-Verlag, Berlin* **1926**.

[8] Versteeg HK and Malalasekera W. An Introduction to Computational Fluid Dynamics, Second Edition. *Pearson* **2007**.

[9] Greenshields CJ and Weller HG. Notes on Computational Fluid Dynamics: General Principles. *CFD Direct Ltd.* **2022**.

[10] Rodriguez S. Applied Computational Fluid Dynamics and Turbulence Modeling. *Springer* **2019**.

[11] Kármán Th. von. Mechanische Ähnlichkeit und Turbulenz. Nachrichten von der Gesellschaft der Wissenschaften zu Göttingen, Mathematisch-Physikalische Klasse **1930**, 58-76 (1930).

[12] Perry AE, Henbest S, Chong MS. A theoretical and experimental study of wall turbulence. J. Fluid Mech. **165**, 163-199 (1986).

[13] Davidson PA and Krogstad P-Å. A simple model for the streamwise fluctuations in the log-law region of a boundary layer. Phys. Fluids **21**, 055105 (2009).

[14] Pope SB. Turbulent Flows. *Cambridge University Press* **2000**.

[15] Apsley DD. Turbulence modelling. [Online]
`https://personalpages.manchester.ac.uk/staff/david.d.apsley/lectures/comphydr/index.htm`
(accessed January 2023)

[16] Boussinesq J. Essai sur la théorie des eaux courantes. Mémoires présentés par divers savants á l'Académie des Sciences **23**, 1-680 (1877).

[17] Kolmogorov AN. The equations of turbulent motion in an incompressible fluid (in Russian). Izvestia Acad. Sci., USSR; Phys. **6**, 56-58 (1942).

[18] Prandtl L. Über ein neues Formelsystem für die ausgebildete Turbulenz. Nachr. Akad. Wiss. Göttingen Math.-Phys. Klasse, 6-19 (1945).

[19] Taylor GI. Statistical theory of turbulence, Parts I-IV. Proc. R. Soc. Lond. A **151**, 421-478 (1935).

[20] Wilcox DC. Turbulence Modeling for CFD, Third Edition. *DCW Industries* **2006**.

[21] Jones WP and Launder BE. The prediction of laminarization with a two-equation model of turbulence. Int. J. Heat Mass Transfer **15**, 301-314 (1972).

[22] Bradshaw P, Ferriss DH and Atwell NP. Calculation of boundary-layer development using the turbulent energy equation. J. Fluid Mech. **28**, 593-616 (1967).

[23] Ansys Fluent User's Guide, Release 2022 R2 (2022).

[24] Tennekes H and Lumley JL. A First Course in Turbulence. *MIT Press* **1972**.

[25] Nikuradse J. Gesetzmäßigkeiten der turbulenten Strömung in Glatten Rohren. VDI Forschungsheft **356**, 1-36 (1932).

[26] Gersten K and Herwig H. Strömungsmechanik. *Springer* **1992**.

[27] Greenshields C. Private Communication (2021).

[28] Basse NT. Extrapolation of turbulence intensity scaling to $Re_\tau \gg 10^5$. Phys. Fluids **34**, 075128 (2022).

[29] Basse NT. Turbulence intensity scaling: A fugue. Fluids **4**, 180 (2019).

[30] Schlichting H and Gersten K. Boundary-Layer Theory, 8th Ed. *Springer* **2000**.

[31] Prandtl L. Der Luftwiderstand von Kugeln. Nachrichten der Gesellschaft der Wissenschaften zu Göttingen. *Springer* **1914**.

[32] Cogo M, Salvadore F, Picano F and Bernardini M. Direct numerical simulation of supersonic and hypersonic turbulent boundary layers at moderate-high Reynolds numbers and isothermal wall condition. J. Fluid Mech. **945**, A30 (2022).

[33] Pirozzoli S, Romero J, Fatica M, Verzicco R and Orlandi P. One-point statistics for turbulent pipe flow up to $Re_\tau \approx 6000$. J. Fluid Mech. **926**, A28 (2021).

[34] Chi C, Thévenin D, Smits AJ, Wolligandt S and Theisel H. Identification and analysis of very-large-scale turbulent motions using multiscale proper orthogonal decomposition. Phys. Rev. Fluids **7**, 084603 (2022).

[35] Smits AJ. Batchelor Prize Lecture: Measurements in wall-bounded turbulence. J. Fluid Mech. **940**, A1 (2022).

[36] Rodi W. The prediction of free turbulent boundary layers by use of a two-equation model of turbulence. Ph.D. thesis, Univerity of London (1972).

[37] Russo F and Basse NT. Scaling of turbulence intensity for low-speed flow in smooth pipes. Flow Meas. Instrum. **52**, 101-114 (2016).

[38] Hanjalić K, Launder BE and Schiestel R. Multiple-time-scale concepts in turbulent transport modelling. In: Turbulent Shear Flows 2, Eds. Bradbury LJS, Durst F, Launder BE, Schmidt FW and Whitelaw JH. *Springer* **1980**.

[39] Klein TS, Craft TJ and Iacovides H. The development and application of two-time-scale turbulence models for non-equilibrium flows. Int. J. Heat Fluid Flow **71**, 334–352 (2018).

[40] Hamlington PE and Ihme M. Modeling of non-equilibrium homogeneous turbulence in rapidly compressed flows. Flow Turbulence Combust. **93**, 93-124 (2014).

[41] Launder BE and Spalding DB. The numerical computation of turbulent flows. Computer Meth. Appl. Mech. Eng. **3**, 269-289 (1974).

[42] Speziale CG. Modeling non-equilibrium turbulent flows. In: Modeling Complex Turbulent Flows, Eds. Salas MD, Hefner JN and Sakell L. *Springer* **1999**.

[43] Zoletnik S, Basse NP, Saffman M, Svendsen W, Endler M, Hirsch M, Werner A, Fuchs Ch and the W7-AS Team. Changes in density fluctuations associated with confinement transitions close to a rational edge rotational transform in the W7-AS stellarator. Plasma Physics and Controlled Fusion **44**, 1581-1607 (2002).

[44] Basse NP, Michelsen PK, Zoletnik S, Saffman M, Endler M and Hirsch M. Spatial distribution of turbulence in the Wendelstein 7-AS stellarator. Plasma Sources Science and Technology **11**, A138-A142 (2002).

[45] Launder BE and Sharma BI. Application of the energy-dissipation model of turbulence to the calculation of flow near a spinning disc. Lett. Heat Mass Transfer **I**, 131-138 (1974).

[46] Hoyas S, Oberlack M, Alcántara-Ávila F, Kraheberger SV and Laux J. Wall turbulence at high friction Reynolds numbers. Phys. Rev. Fluids **7**, 014602 (2022).

[47] Yao J, Chen X and Hussain F. Direct numerical simulation of turbulent open channel flows at moderately high Reynolds numbers. J. Fluid Mech. **953**, A19 (2022).

[48] Pope SB. A more general effective-viscosity hypothesis. J. Fluid Mech. **72**, 331-340 (1975).